AD-A236 073

WRDC-TR-90-5032

COMPENSATING-STRESS InAs QUANTUM WELLS FOR HIGH-PERFORMANCE ELECTRONIC DEVICES

C.W. Tu
University of California, San Diego
Department of Electrical and Computer Engineering
La Jolla, CA 92093-0407

NOVEMBER 1990

Final Report for Period: September 1988 - September 1990

Approved for public release; distribution unlimited.

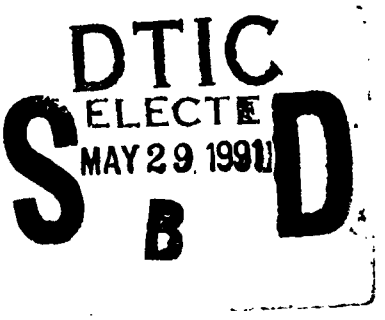

ELECTRONIC TECHNOLOGY LABORATORY
WRIGHT RESEARCH AND DEVELOPMENT CENTER
AIR FORCE SYSTEMS COMMAND
WRIGHT-PATTERSON AIR FORCE BASE, OHIO 45433-6543

91-00538

91 5 24 060

NOTICE

WHEN GOVERNMENT DRAWINGS, SPECIFICATIONS, OR OTHER DATA ARE USED FOR ANY PURPOSE OTHER THAN IN CONNECTION WITH A DEFINITELY GOVERNMENT-RELATED PROCUREMENT, THE UNITED STATES GOVERNMENT INCURS NO RESPONSIBILITY OR ANY OBLIGATION WHATSOEVER. THE FACT THAT THE GOVERNMENT MAY HAVE FORMULATED OR IN ANY WAY SUPPLIED THE SAID DRAWINGS, SPECIFICATIONS, OR OTHER DATA, IS NOT TO BE REGARDED BY IMPLICATION, OR OTHERWISE IN any MANNER CONSTRUED, AS LICENSING THE HOLDER, OR ANY OTHER PERSON OR CORPORATION; OR AS CONVEYING ANY RIGHTS OR PERMISSION TO MANUFACTURE, USE, OR SELL ANY PATENTED INVENTION THAT MAY IN ANY WAY BE RELATED THERETO.

THIS REPORT IS RELEASABLE TO THE NATIONAL TECHNICAL INFORMATION SERVICE (NTIS). AT NTIS IT WILL BE AVAILABLE TO THE GENERAL PUBLIC, INCLUDING FOREIGN NATIONS.

THIS TECHNICAL REPORT HAS BEEN REVIEWED AND IS APPROVED FOR PUBLICATION.

Paul E. Cook

PAUL E. COOK, Capt, Project Engineer
Device Research Branch
Research Division

Fritz Schuermeyer

FRITZ SCHUERMEYER, Acting Chief
Device Technology Branch
Microelectronics Division

FOR THE COMMANDER

Stanley E. Wagner

Stanley E. Wagner, Chief
Microelectronics Division
Electronic Technology Laboratory

IF YOUR ADDRESS HAS CHANGED, IF YOU WISH TO BE REMOVED FROM OUR MAILING LIST, OR IF THE ADDRESSEE IS NO LONGER EMPLOYED BY YOUR ORGANIZATION PLEASE NOTIFY WL/ELRD , WRIGHT-PATTERSON AFB, OH 45433-6543 TO HELP MAINTAIN A CURRENT MAILING LIST.

COPIES OF THIS REPORT SHOULD NOT BE RETURNED UNLESS RETURN IS REQUIRED BY SECURITY CONSIDERATIONS, CONTRACTUAL OBLIGATIONS, OR NOTICE ON A SPECIFIC DOCUMENT.

Unclassified

CURITY CLASSIFICATION OF THIS PAGE

REPORT DOCUMENTATION PAGE

Form Approved
OMB No. 0704-0188

. REPORT SECURITY CLASSIFICATION UNCLASSIFIED	1b. RESTRICTIVE MARKINGS
. SECURITY CLASSIFICATION AUTHORITY	3. DISTRIBUTION / AVAILABILITY OF REPORT approved for public release; distribution is unlimited.
. DECLASSIFICATION / DOWNGRADING SCHEDULE	
PERFORMING ORGANIZATION REPORT NUMBER(S) TU-WRDC-90	5. MONITORING ORGANIZATION REPORT NUMBER(S) WRDC-TR-90-5032
. NAME OF PERFORMING ORGANIZATION Univ. Calif. San Diego 6b. OFFICE SYMBOL (If applicable)	7a. NAME OF MONITORING ORGANIZATION Wright REsearch and Development Center Avionics Laboratory /WRDC/ELRD
. ADDRESS (City, State, and ZIP Code) Dept. Electrical & Computer Engineering 0407 La Jolla, CA 92093-0407	7b. ADDRESS (City, State, and ZIP Code) Wright Patterson AFB OH 45433-6543
a. NAME OF FUNDING / SPONSORING ORGANIZATION 8b. OFFICE SYMBOL (If applicable)	9. PROCUREMENT INSTRUMENT IDENTIFICATION NUMBER F33615-88-C-1861
c. ADDRESS (City, State, and ZIP Code)	10. SOURCE OF FUNDING NUMBERS

PROGRAM ELEMENT NO.	PROJECT NO.	TASK NO	WORK UNIT ACCESSION NO.
61106F	ILIR	A8	08

1. TITLE (Include Security Classification)

Compensating-Stress InAs Quantum Wells for High-Performance Electronic Devices

2. PERSONAL AUTHOR(S)
C.W. Tu

3a. TYPE OF REPORT	13b. TIME COVERED	14. DATE OF REPORT (Year, Month, Day)	15. PAGE COUNT
Final	FROM 9/88 TO 9/90	1990 November 29	80

6. SUPPLEMENTARY NOTATION
This research was partially funded by the Inhouse Independent Research Fund.

7. COSATI CODES			18. SUBJECT TERMS (Continue on reverse if necessary and identify by block number)
FIELD	GROUP	SUB-GROUP	MBE, gas-source MBE, InGaAs, AlGa As, GaAs, InAs, InP, InAlAs, pseudomorphic MODFET.
09	03		

9. ABSTRACT (Continue on reverse if necessary and identify by block number)

In this contract we have investigated various approaches of compensating stress to increase the InAs molar fraction in an InGaAs-channel MODFET. Conventional solid-source MBE and hydride-source MBE were used. Key accomplishments included:

- Establishing a baseline AlGaAs/InGaAs pseudomorphic MODFET technology.
- Using an $(InAs)_2(GaAs)_2$ superlattice grown by migration-enhanced epitaxy at 400°C as the channel layer of a MODFET (with effective InAs molar fraction of 0.5) results in better luminescence properties and device performance than MBE-grown random-alloy $In_{0.4}Ga_{0.6}As$ as the channel layer.
- Setting up a gas-source MBE system with elemental group-III and doping sources and arsine and phosphine.
- Establishing precisely the V/III atomic ratio on the growing surface during gas-source MBE by using the RHEED oscillation techniuqe in the group-V-limited growth mode.
- Obtaining some preliminary results on modulation-doped, pseudomorphic InGaP/InGaAs.

0. DISTRIBUTION / AVAILABILITY OF ABSTRACT	21. ABSTRACT SECURITY CLASSIFICATION
☒ UNCLASSIFIED/UNLIMITED ☐ SAME AS RPT. ☐ DTIC USERS	UNCLASSIFIED

2a. NAME OF RESPONSIBLE INDIVIDUAL	22b. TELEPHONE (Include Area Code)	22c. OFFICE SYMBOL
Paul Cook	(513)255-8627	WRDC/ELRD

D Form 1473, JUN 86 *Previous editions are obsolete.* SECURITY CLASSIFICATION OF THIS PAGE
UNCLASSIFIED

TABLE OF CONTENTS

Accession For
NTIS GRA&I ☑
DTIC TAB ☐
Unannounced ☐
Justification
By
Distribution/
Availability Codes
Dist | Avail and/or Special
A-1

LIST OF FIGURES

EXECUTIVE SUMMARY

This final report details the growth and characterization of modulation-doped structures with InGaAs channels having InAs molar fractions from 0 to 0.5. Two types of large-bandgap, electron-supplying layers were used; one being arsenides (AlGaAs) and the other, phosphides (InGaP). Compensating-stress approach was employed for both types of structures in different ways. For the AlGaAs case, $(InAs)_n$ $(GaAs)_m$ monolayer superlattices for the channel region were investigated. For the InGaP case, compensated-stress InGaP/InGaAs layers were grown. For AlGaAs/InGaAs modulation-doped structures we also present device fabrication and testing results.

We first present luminescent and device properties of pseudomorphic AlGaAs/InGaAs modulation-doped field-effect transistors (MODFET's) with different InAs molar fractions in the InGaAs channel. Molecular-beam epitaxy (MBE), which simultaneously deposits group-III atoms and As_4 molecules on the substrate surface, was used to grow random alloy $In_xGa_{1-x}As$ channel layers for $x \leq 0.4$, and migration-enhanced epitaxy (MEE), which alternatingly deposits group-III atoms and As_4 molecules on the surface, was used to grow sequential layers of InAs and GaAs in the channel region with large effective x (<0.5). For 1-micron-gate-length MODFET's with random-alloy $In_xGa_{1-x}As$ channels the transconductance g_m and saturation drain current I_{dss} exhibit a maximum at x=0.17 because of superior electron transport properties of InGaAs than GaAs. g_m and I_{dss} decrease drastically for x larger than 0.32 because of misfit dislocation generation. The photoluminescence peaks of $In_xGa_{1-x}As$ channels of these MODFET samples show a similar trend, strong intensity for the $In_{0.17}Ga_{0.83}As$ channel and very weak intensity for the $In_{0.4}Ga_{0.6}As$ channel. However, MODFET's with a nominally $(InAs)_2(GaAs)_2$ channel grown by MEE exhibit higher g_m, I_{dss}, and photoluminescence intensity than those with an $In_{0.4}Ga_{0.6}As$ channel.

Then we present results involving phosphides. We have to set up a gas-source MBE system with a combination of group-III solid sources and group-V hydride sources. We first optimized the growth of various phosphides, GaP, AlP, and InP, with particular emphasis on InP. We then studied interfacial properties of heterostructures with different group-V elements in adjacent layers. Finally we present Hall data of selectively doped n-InGaP/InGaAs structures.

In Appendix B, we present some results that are relevant to p-channel pseudomorphic MODFET's and list conference presentations and publications that were partially supported by this contract.

1. INTRODUCTION

Pseudomorphic AlGaAs/$In_xGa_{1-x}As$ modulation-doped field-effect transistors (MODFET's) have attracted considerable attention recently for high-speed integrated circuit (IC) and microwave applications[1,2] because $In_xGa_{1-x}As$ has a smaller electron effective mass, higher electron velocity and smaller energy bandgap than GaAs. The lattice mismatch between $In_xGa_{1-x}As$ and GaAs must be chosen within a critical limit (which depends on x and on thickness of $In_xGa_{1-x}As$ layer) so that no misfit defects are generated.[2,3] Typically, the $In_xGa_{1-x}As$ channel thicknesses of 100 - 200 Å and InAs molar fractions $x \leq 0.25$ are used in order to maintain a coherent interfacial strain and a pseudomorphic deformation of the crystal lattice in the active channel. For higher InAs molar fractions the channel thickness should be reduced, but the electron confinement potential is reduced because of the quantum-size effect. The goal of the contract is to see whether a compensated-stress approach can allow higher InAs molar fractions while ~150 Å of the channel layer is maintained.

In the first part we describe our investigation of higher InAs molar fractions in the MODFET channel. Large indium concentration in the $In_xGa_{1-x}As$ ternary alloy might provide better charge carrier transport properties and stronger electron confinement. We report here growth, characterization and device performance of $Al_{0.28}Ga_{0.72}As/In_xGa_{1-x}As/Al_{0.28}Ga_{0.72}As$ MODFET's with x up to 0.5. Both molecular-beam epitaxy (MBE) of random alloy $In_xGa_{1-x}As$ and migration-enhanced epitaxy (MEE) of alternating deposition of InAs and GaAs are compared. The MEE technique results in better luminescent and device properties for high In concentration in the active layer.

In the second part we describe the set up of a new gas-source MBE system for growing phosphorus- and arsenic-containing compounds. We then discuss various issues in optimized growth conditions and interfacial properties involving As and P, and present preliminary results on compensated-stress InGaP/InGaAs modulation-doped structures.

2. ARSENIDE-BASED MODFET HETEROSTRUCTURES

2.1 Establish a Baseline MODFET Technology

In the beginning we had to establish a base-line technology on MBE and MODFET's. We have optimized the growth conditions of GaAs, InGaAs, and AlGaAs layers in uniformly doped and δ-doped (planar-doped) MODFET structures and have established fabrication process of 1-μm gate length MODFET's at UCSD.

MODFET's are fabricated using a recessed-gate technology. Mesas are defined by means of photolithography and a H_3PO_4:H_2O_2:H_2O (1:1:25) etch. The source-drain ohmic contact metallurgy consists of 1000Å Au:Ge eutectic and 150 Å Ni. The contacts are alloyed at 430°C for 30 sec under forming gas flow. Following the source-drain ohmic contact formation, a NH_4OH:H_2O_2 (pH =7) selective etchant is used for the recessed gate etching. Finally, 3000 Å of Al is deposited to form the gate/contact pad.

The growth sequence of the MODFET structure, shown in Figure 1, was as follows: (1) 2000 Å GaAs buffer and 20 periods of $Al_{0.28}Ga_{0.72}As$(200 Å)/GaAs(15 Å) multiple quantum well (MQW); (2) a delta-doped region in the $Al_{0.28}Ga_{0.72}As$ layer with a Si sheet concentration of $2x10^{12}$ cm^{-2}, followed by a 20 Å $Al_{0.28}Ga_{0.72}As$ spacer and a 30 Å GaAs layer to provide a smooth surface; (3) a 150 Å InGaAs channel, the thickness of which is kept constant throughout the experiment; (4) a top delta-doped region in an $Al_{0.28}Ga_{0.72}As$ layer with a Si sheet doping concentration of $6x10^{12}$ cm^{-2} spaced 30Å from the InGaAs channel; (5) a 300 Å Si-doped $Al_{0.28}Ga_{0.72}As$ with a doping concentration of 10^{17} cm^{-3}; and (6) a 400 Å GaAs contact layer with a doping concentration of $4x10^{18}$ cm^{-3}. The growth rate and alloy composition were calibrated by the RHEED intensity oscillations.

The MQW buffer is intended to smooth out surface irregularities, to reduce impurity out-diffusion from the substrate to provide better carrier confinement, and to reduce output conductance. The top AlGaAs layer is lightly doped to 10^{17} cm^{-3} to reduce the possibility of parallel conduction in the AlGaAs layer and to increase the breakdown voltage compared to conventional, heavily doped AlGaAs electron-suppling layers. The delta-doping technique increases the two-dimensional electron concentration in the channel.[4] In order to increase the sheet electron density of the channel even more,[5] we introduced two delta-doped regions on each side of the

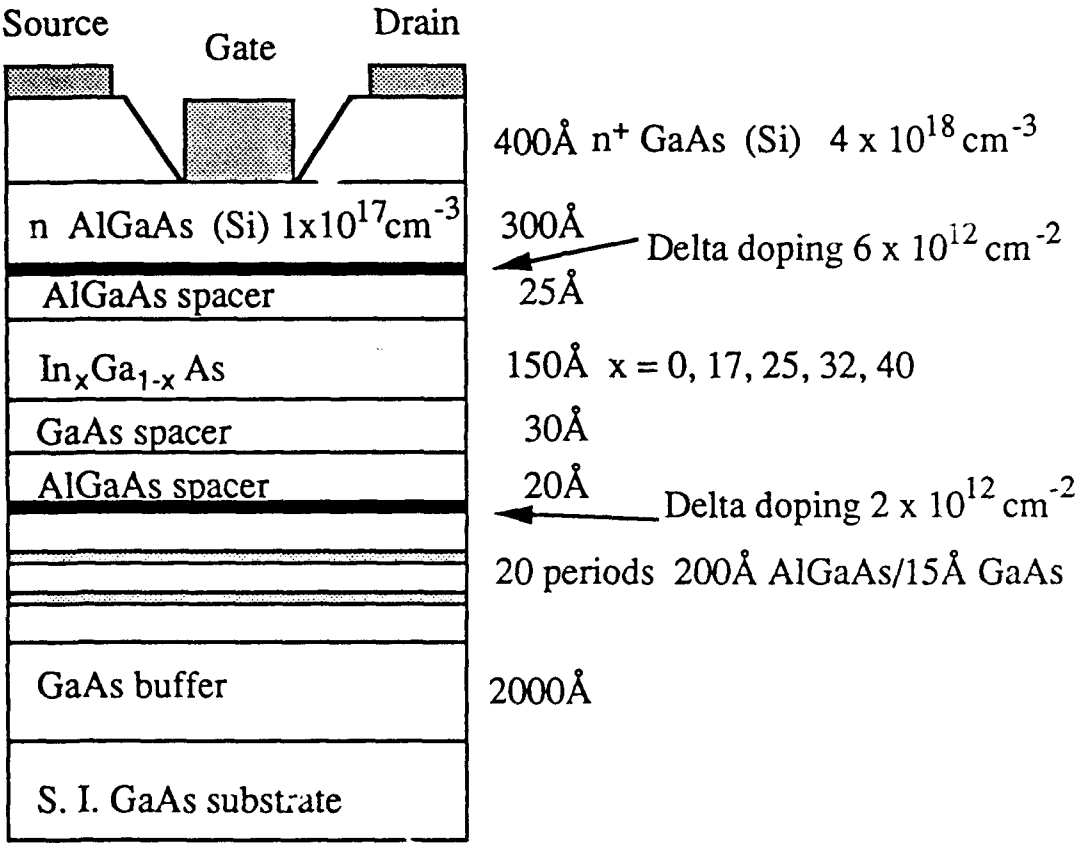

Figure 1 Schematic diagram of our baseline MODFET structure.

channel. Hall measurement gives a sheet carrier concentration of about $4x10^{12}$ cm^{-2}.

We have investigated the optimal InAs molar fraction in pseudomorphic MODFETs. We have established the upper limit of the indium molar fraction in our pseudomorphic AlGaAs/InGaAs/AlGaAs MODFET structure with a 150 Å channel layer thickness. Indium content exceeding the upper limit of 25-30% leads to degradation in the saturation channel current and results in lower FET transconductance. The degradation in electrical performance characteristics was traced to poor device material quality and confirmed by data obtained from photoluminescence measurements. Figure 2 shows the transistor characteristics of one of the best devices with 17% In in the channel. For 1-μm gate length the transconductance is 342 mS/mm and the saturation current, measured at gate voltage of 1 V, is 450 mA/mm. The breakdown voltage is 11-13 V. Figure 3 shows the microwave performance of this device. The unity-current-gain cut-off frequency (f_t) is 19 GHz, whereas the maximum frequency of oscillation (f_{max}) is 60 GHz. As a comparison, the AlGaAs/GaAs MODFET has a f_{max} of 43 GHz. The gain of the device versus frequency is obtained from measured s-parameter data. A small-signal equivalent circuit of the device, which provides an idea of the prarasitics of the device, was also derived from the s-parameter data using the software package Touchstone and is shown in Figure 4. These data demonstrate that at UCSD we have established a meaningful baseline technology with results comparable to elsewhere in the world using the same recess-gate 1-μm technology.

In addition, Dr. C.S. Wu and his co-workers at Hughes Aircraft Co., Torrance, California, using our materials, have fabricated MODFET's with 0.25-μm gate length. Transconductance of 430 mS/mm and I_{dss} of 600 mA/mm are obtained, as shown in Figure 5. The f_t is measured to be 55 GHz, and the f_{max} is expected to be well over 100 GHz. The Hughes engineers have also observed increasing power output with increasing In concentration. All of these results point to the superior properties of a pseudomorphic δ-doped MODFET.

2.2 InAlAs/InGaAs

Tsui and his coworkers have reported that the effective mass of a strained InGaAs is not as small as that of an unstrained layer.[6] Therefore, it would be advantageous to take potential advantages of even higher In concentration in an unstrained channel by decoupling the active layers from the substrate. We first

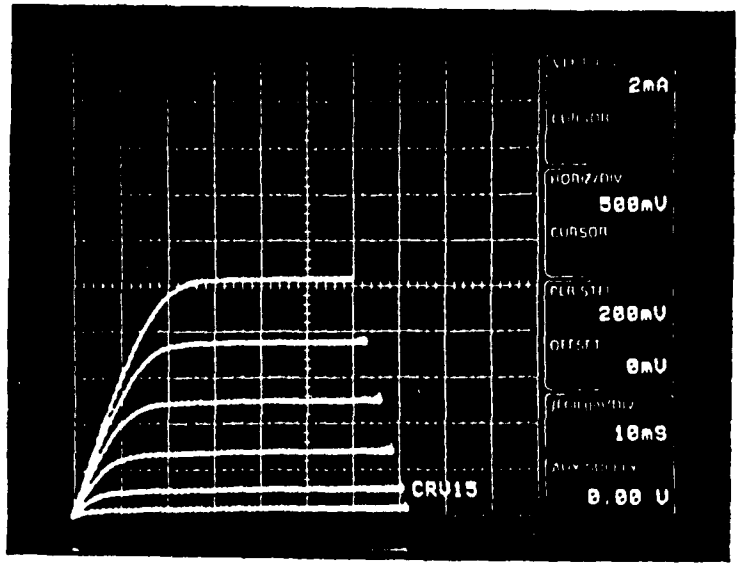

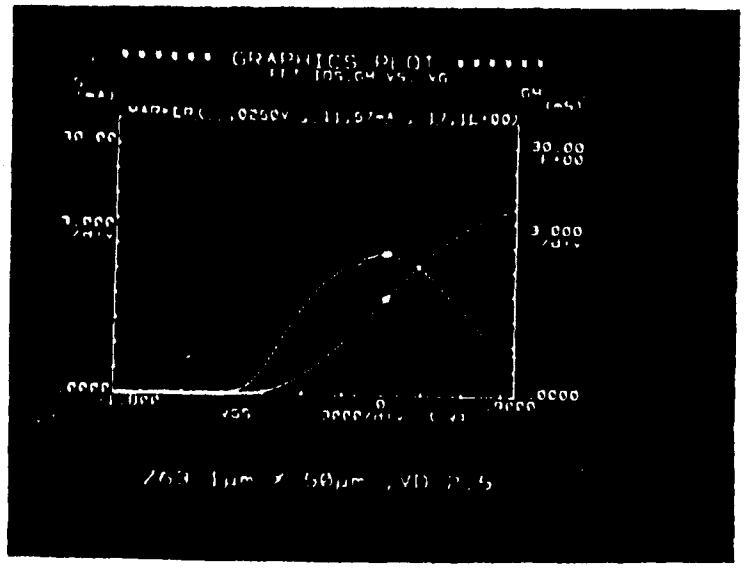

Transconductance = 342mS/mm

Idss (at Vg = 1.0V) = 450 mA/mm

Breakdown Voltage = 11 - 13V

Figure 2 I-V characteristics of a pseudomorphic AlGaAs/InGaAs MODFET with 17% InAs molar fraction in the channel.

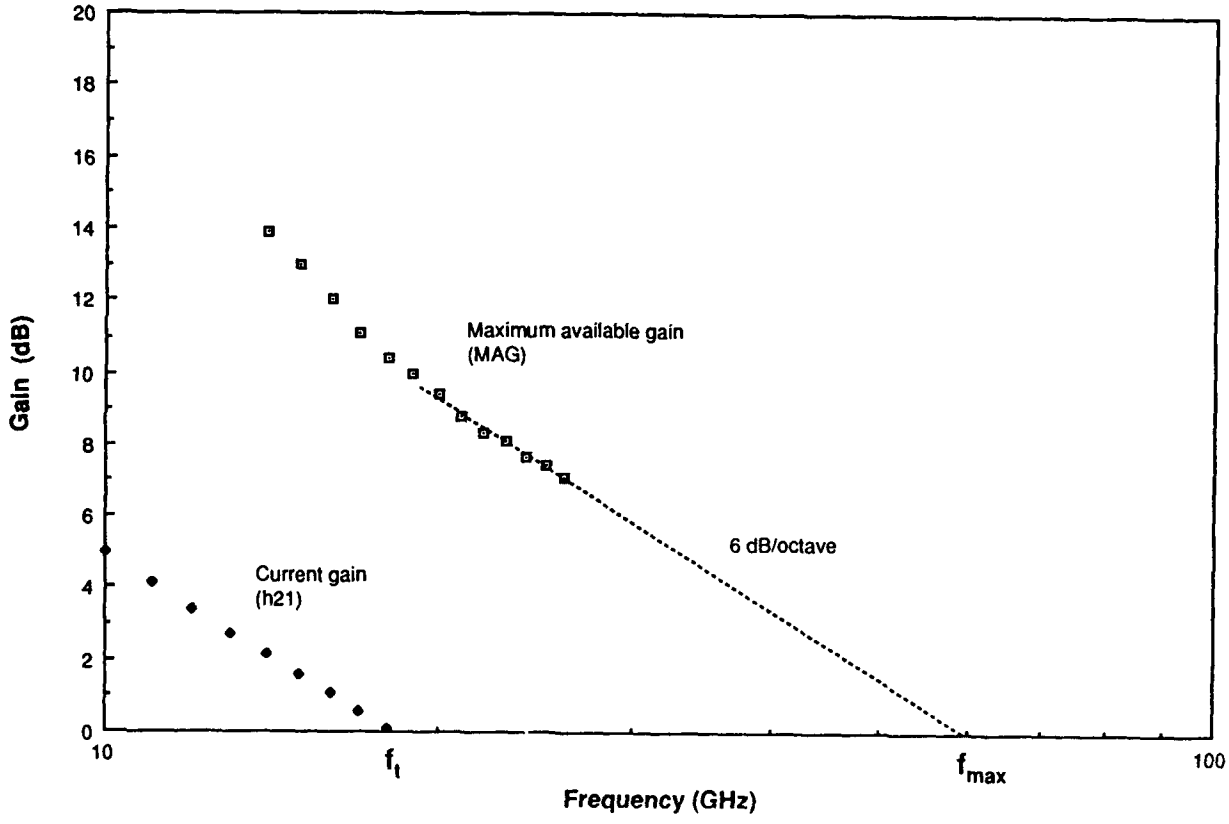

Figure 3 Microwave measurement of the MODFET of Figure 2. The unity-current-gain cut-off frequency (f_t) is 19 GHz, and the maximum frequency of oscillation (f_{max}) is 60 GHz.

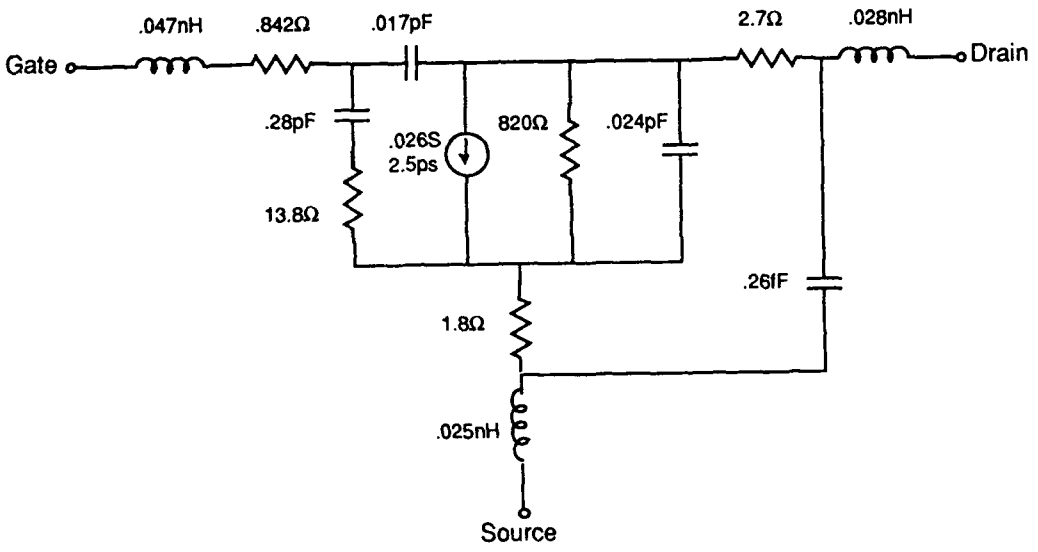

Figure 4 Small-signal equivalent circuit model of the MODFET of Figure 2

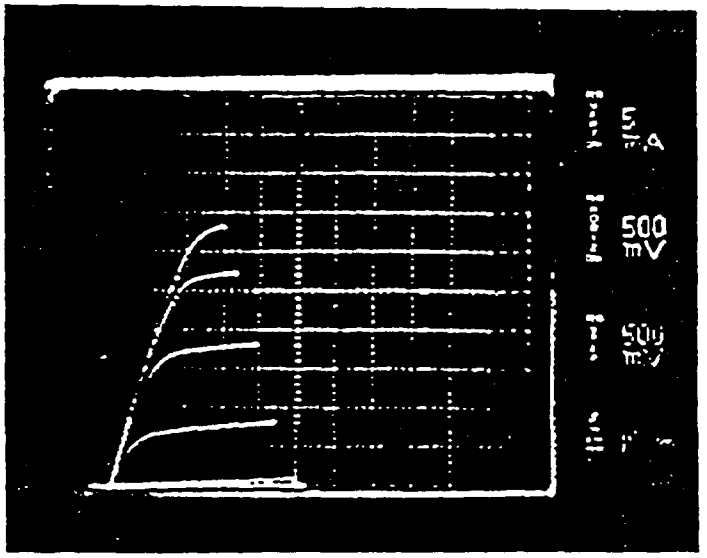

vertical
5 mA

horizontal
500 mV

per step
50 mV

Z041

L_g = 0.25 μm

W_g = 53 μm

g_m = 433 mS/mm

I_{dss} = 632 mA/mm

Figure 5 I-V characteristics of a 0.25 μm-gate-length pseudomorphic AlGaAs/InGaAs MODFET with 20% InAs in the channel. f_t is 55 GHz.

investigated a number of unstrained $In_{0.39}Al_{0.61}As/In_{0.40}Ga_{0.60}As$ structures on an $In_{0.39}Al_{0.61}As$ buffer, which is lattice-mismatched to a GaAs substrate. The structure is shown in Figure 6. Different InAlAs/InAlAs strained layer superlattices were used as dislocation filtering layers. (The reason for using InAlAs instead of InGaAs is to have better channel confinement.) Figure 7 shows the calculation of the strain (lattice mismatch) and the critical layer thickness h_c as a function of In composition with respect to $In_{0.39}Al_{0.61}As$. The calculation was done according to the Matthews and Blakeslee theory.[2] Sample Z009 is an $In_{0.35}Al_{0.65}As/In_{0.28}$-$Ga_{0.72}As$ strained layer superlattice with strain of + 0.20% and – 0.28% with respect to the buffer layer of $In_{0.32}Al_{0.68}As$. The buffer layer composition is not the targeted 40% because at that time we did not use RHEED to calibrate the growth rate and composition before growth. Dr. George Chu of AT&T Bell Laboratories at Murray Hill, NJ, took a cross-section transmission electron micrograph (TEM) of the sample, as shown in Figure 8. First, because this sample has no GaAs smoothing buffer layer and perhaps the growth initiation was not optimal, the surface is not smooth. The InAlAs buffer layer and the SLS basically follow the topology of the substrate surface. The SLS does not seem effective in blocking threading dislocation propagation. Many stacking faults are also present.

Nevertheless, we proceeded to calibrate doping concentrations for the n-$In_{0.40}Ga_{0.60}As$ cap layer and the n-$In_{0.39}Al_{0.61}As$ donor layer in an InAlAs/InGaAs MODFET structure. The InGaAs and InAlAs layers are 2500 Å each on top of a 1 μm $In_{0.39}Al_{0.61}As$ buffer layer. We find that for a given Si flux, the free carrier concentration, as measured by Hall measurements, for InGaAs is 1.2X18 cm^{-3}, and for InAlAs it is 6.7X17 cm^{-3}. The difference is due to different ionization energies of Si in InGaAs and in InAlAs. The mobilities are about 1000 and 200 cm^2/Vs, respectively. They are about a factor of three to four lower than mobilities for comparably doped $In_{0.53}Ga_{0.47}As$ and $In_{0.52}Al_{0.48}As$ latticed-matched to InP substrates. We grew a MODFET structure, as shown in Figure 6. The undoped InGaAs cap was used so that we did not have to etch the doped cap layer for the Hall measurement. The InAlAs spacer layer is 10 nm to obtain more clearly the mobility enhancement. (Such a structure with an undoped cap and a relatively thick spacer layer is generally used in ion-implantation technology for MODFET's.) The room temperature Hall measurements show a sheet carrier density of 1.6X12 cm^{-2} and a mobility of 3,600 cm^2/Vs. There is little difference between measurements in the dark or under room light illumination. Compared to the 2DEG mobility in a lattice-matched structure on InP substrate (with an $In_{0.53}Ga_{0.47}As$ active layer), our mobility is about a factor

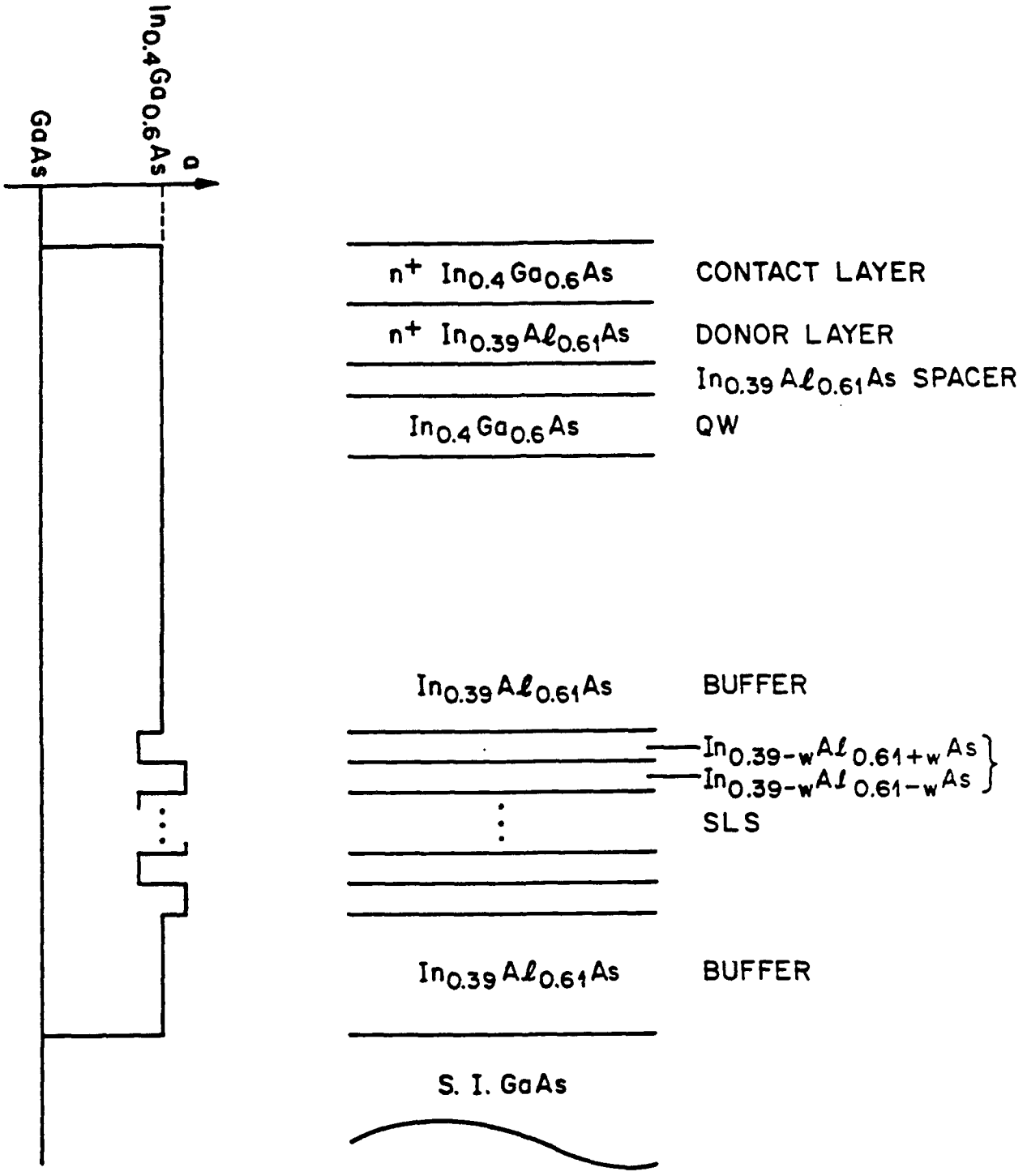

Figure 6 An AlInAs/InGaAs MODFET structure on a GaAs substrate.

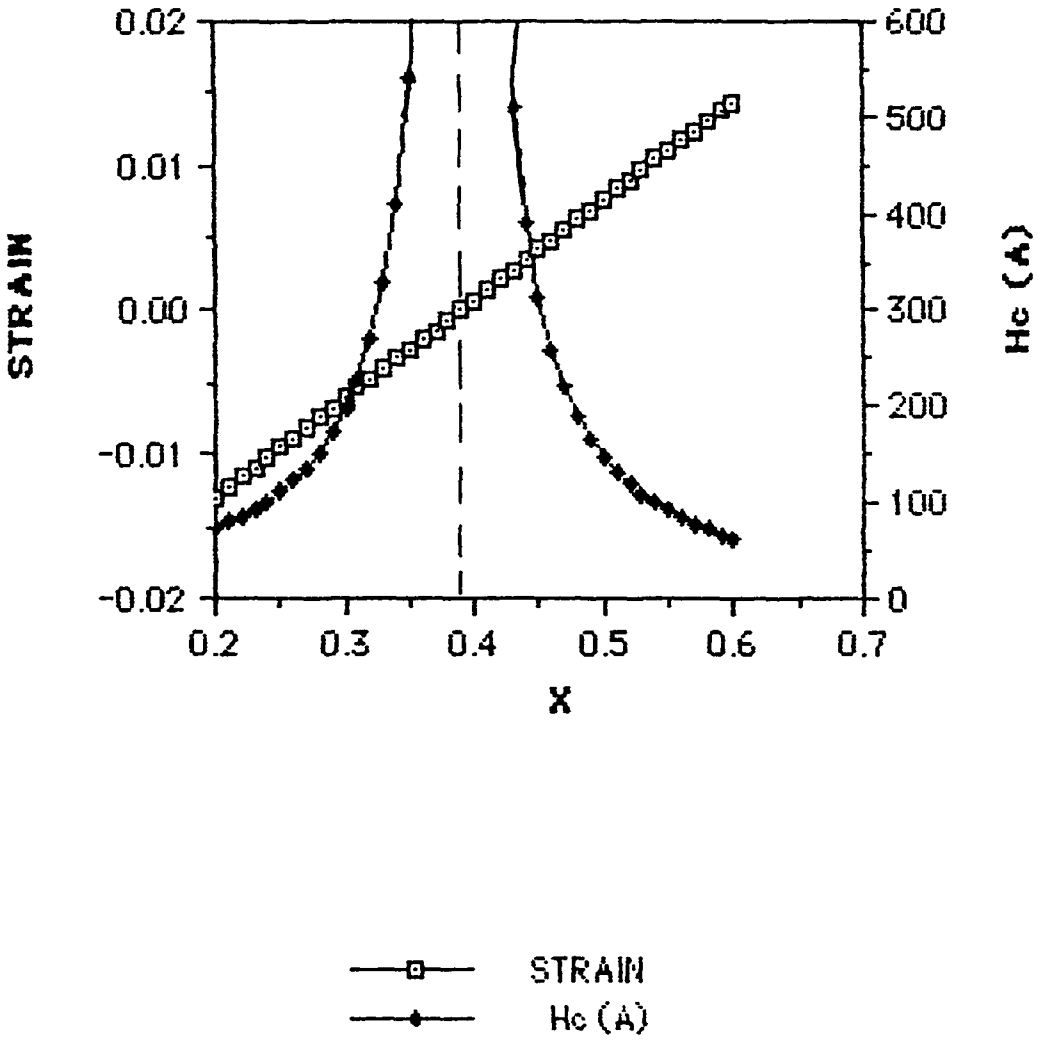

Figure 7 Strain (lattice-mismatch) and critical layer thickness (h_c) as a function of InAs molar fraction x with respect to $In_{0.39}Al_{0.61}As$. The calculation is according to the Matthews and Blakeslee theory.

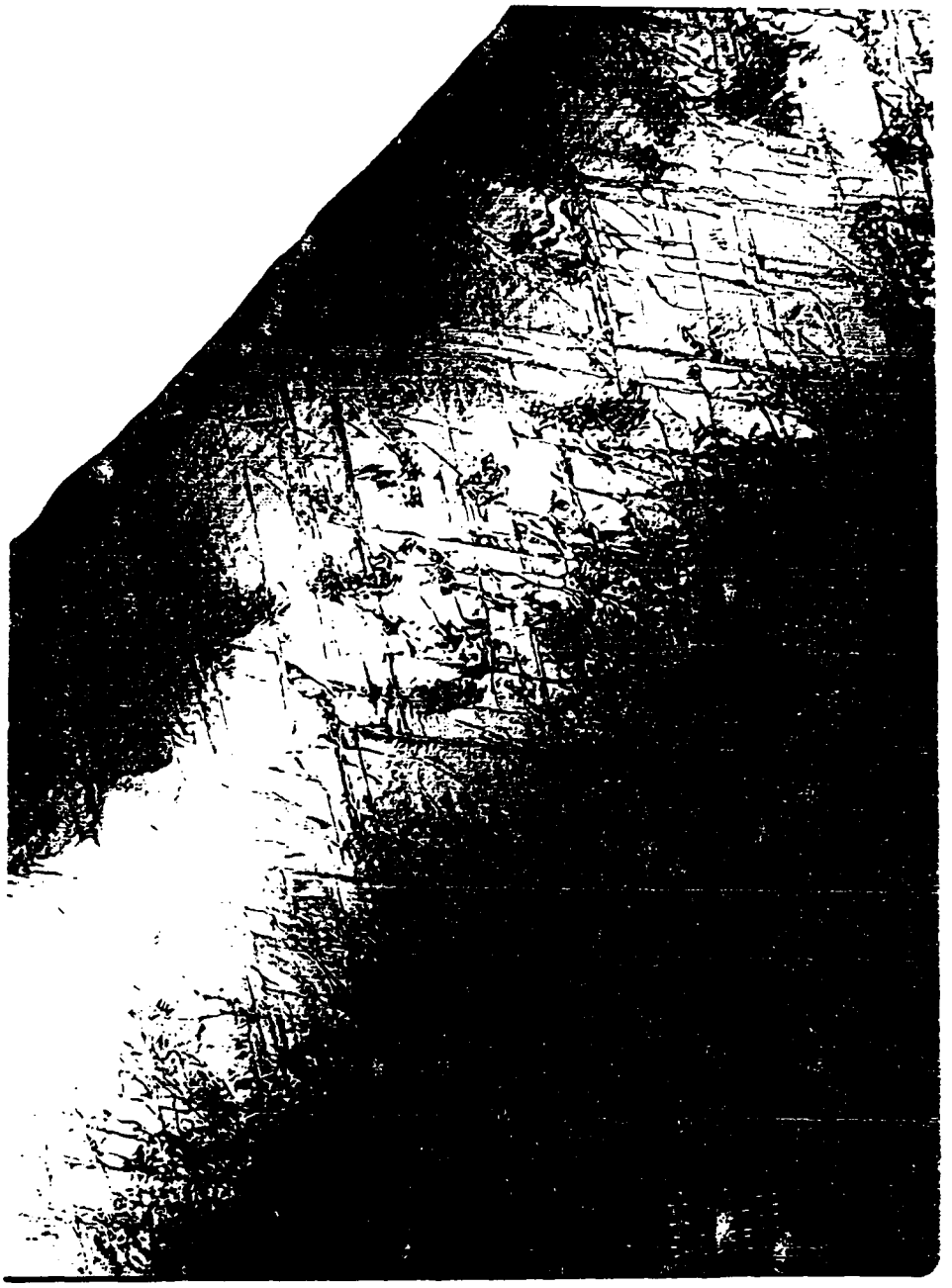

Figure 8 Cross-section TEM micrograph of sample Z009, $In_{0.35}Al_{0.65}As/In_{0.28}Al_{0.72}AS$ SLS on a 1 mm $In_{0.32}Ga_{0.68}As$ buffer layer on GaAs(100). The magnification is 49,000.

of three worse. Nevertheless, it is an encouraging result.

Two wafers with MODFET structures were fabricated into devices. The structure and the transistor characteristics are shown in Figure 9. We see looping behavior because of traps. The transconductance was measured to be 65 mS/mm. Since we chose InAlAs as a buffer layer to reduce substrate or buffer conduction, we have another wafer processed by Dr. C.S. Wu at Hughes, Torrance, CA. The buffer breakdown voltage is measured to be greater than 200 V for leakage current of less than 20 μA between two devices separated by 50 μm. As a comparison, a typical breakdown voltage is between 100 and 150 V for GaAs buffer layers. Figure 10 shows the transistor characteristics of the device. The transconductance is 90 mS/mm for 1 μm gate length. The I_{dss} is only 110 mA/mm because the cap layer is only 200 Å. The problem of these devices is the large gate leakage current because our structure and materials were not optimized. Because of these problems and high dislocation density, we stopped working on InAlAs/InGaAs structures and proceeded to work on using compensating stress in the channel to increase the critical layer thickness for large InAs molar fraction.

Recently Ribas et al. have grown high-quality $In_{0.40}Ga_{0.60}As$ epilayers on GaAs, using an elaborately designed multistate strain-relief InGaAs/InAlAs buffer system to control propagation of dislocations.[4]

2.3 Migration-Enhanced Epitaxy (MEE) of InAs

We then turned our attention to growing channel layers with high InAs molar fractions on an AlGaAs buffer layer. Since random alloys of InGaAs grown by conventional MBE show degradation of device performance for x greater than 30%, we decide to look into $(InAs)_n(GaAs)_m$ monolayer superlattice with stress in each layer either tensile or compressive. However, InAs needs to be grown at low substrate temperature to prevent In re-evaporation.[7] Therefore, GaAs has to be grown at the same low substrate temperature. To obtain comparable quality as high-temperature sample, migration-enhanced epitaxy (MEE) has to be used. The following is a discussion on how we performed MEE of InAs.Migration-enhanced epitaxy (MEE) technique has been successfully employed to grow GaAs and AlGaAs epilayers.[8-10] In this technique, group III and V elements are alternatingly deposited onto a substrate. Because of the longer migration length of group-III atoms in the absence of arsenic overpressure, high-quality GaAs and AlGaAs have been achieved

Z # 34 3/30/89

MODFET InAlAs(0.39)/InGaAs(0.40)

n+ InGaAs (x=0.4)	200Å	doped cap layer
n-InAlAs (x=0.39)	300Å	donor layer
InAlAs (x=0.39)	100Å	spacer
InGaAs (x=0.40)	200Å	QW

InAlAs x=0.39	10000Å	
	80Å 80Å	SLS 20 InAlAs (x=0.46) InAlAs (x=0.32)
InAlAs (x=0.39)	6800Å	
GaAs (580C)	3000Å	
S.I. GaAs substrate		

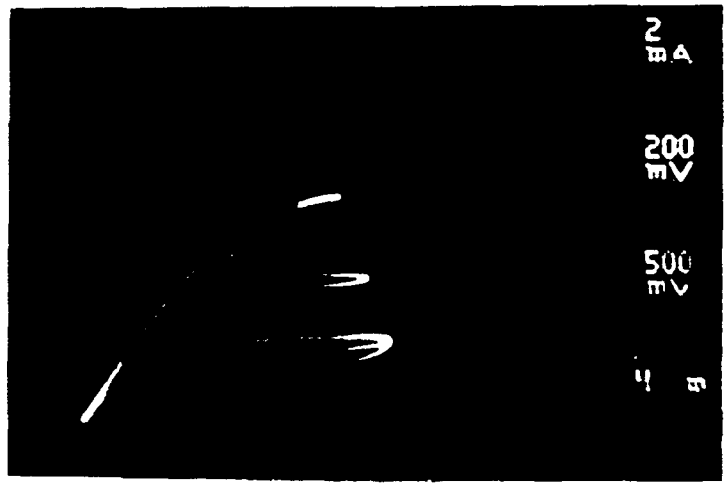

vertical
2 mA

horizontal
200 mV

per step
500 mV

Figure 9 I-V characteristics of the MODFET shown in Figure 6, fabricated at UCSD.

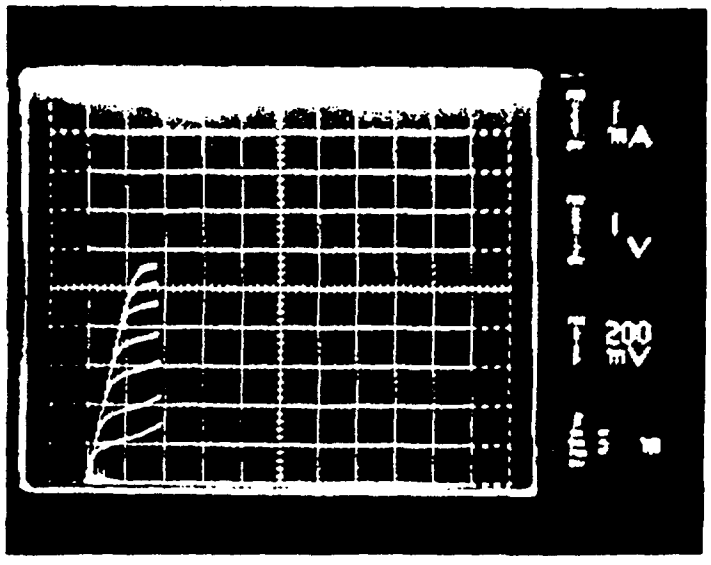

vertical
1 mA

horizontal
1 V

per step
200 mV

Figure 10 I-V characteristics of the MODFET shown in Figure 6, fabricated at Hughes Aircraft Co., Torrance, CA.

at relatively lower substrate temperature. For strained layer epitaxy, MEE experimental results also revealed some improvement in epilayer quality.[11,12]

InAs strained epilayers and InAs/GaAs multiple quantum wells have been grown by MBE.[13-16] The lattice mismatch between the two materials (7.2%) makes epitaxial growth difficult. Strained-layer superlattices, such as InGaAs/GaAs, inserted between InAs and GaAs substrate have been proven important for high-quality epilayers.[15] In this section, we report on the growth of InAs epitaxial layers on GaAs (001) substrate under various conditions. Reflection high-energy-electron diffraction (RHEED) patterns were studied and persistent RHEED oscillations were observed during MEE growth of InAs. The samples were characterized with Hall effect measurement and x-ray rocking curve analysis. We present details of the experimental procedures in the next section, then compare properties of InAs grown by MEE and MBE.

2.3.1 Experimental procedures

Growth was performed in a modified prototype Perkin-Elmer 425A MBE system. The growth chamber was pumped by a cryopump and an ion pump. Either arsenic or indium furnace was opened or closed alternatingly by a single motor-controlled rotary shutter. The on-off frequency of the shutter was controlled with a DC power supply. GaAs (001) wafers were used as the substrates. They were etched and cleaned in the usual manner and then In-mounted on molybdium blocks. The substrate was thermally cleaned at 610°C in vacuum under an overpressure of arsenic. Then, a 1000 Å GaAs buffer layer was grown at 580°C. The substrate temperature was then decreased to 550°C and a 500-Å-thick composition-graded $In_xGa_{1-x}As$ (x from 0 to 0.5) layer, followed by a 5-period InAs(50 Å)/GaAs(25 Å) superlattice at 510°C, was grown via MBE. Then, the substrate temperature was decreased to different InAs growth temperatures, while the arsenic-cell shutter was closed. Typical beam equivalent pressure at the substrate for In is estimated to be $2x10^{-6}$ torr. The As_4 beam-equivalent pressure is $4x10^{-6}$ torr for MEE and $2x10^{-5}$ torr for MBE.

2.3.2 Results and discussion

During MEE of InAs at 400°C the RHEED pattern was a typical As-stablized (2 x 4) surface reconstruction along the [110] azimuth when the As_4 effusion cell was opened but In effusion cell was closed, When the In effusion cell was opened but the As_4 effusion cell was closed, the pattern changed instantaneously to an In-stablized

(4 x 2) surface reconstruction along the same azimuth. Figure 11 shows typical RHEED intensity oscillations during MBE of InAs for different arsenic overpressures. With increasing As_4 overpressure the RHEED intensity increases first at commencement of growth. Before the In cell was opened, excess arsenic molecules accumulated on the substrate surface, and when In was deposited on the substrate surface, these excess arsenic molecules were removed through reaction with In, resulting in smoother growth front and higher RHEED intensity. The key factors for MEE are therefore relative group-III and group-V beam fluxes and deposition duration for both In and As_4.

Figure 12 shows persistent RHEED intensity oscillation when the shutter on-off frequency was low (a period of 5 seconds) and $P_{In} = 1.8 \times 10^{-6}$ torr, $P_{As} = 3.2 \times 10^{-6}$ torr. This As_4 overpressure was higher than optimal. In region (1), when the arsenic effusion cell was opened, RHEED intensity increased, as in Figure 10. Then, it decreased a little because of some more arsenic accumulating on the surface at such low temperature. When In was opened and arsenic was closed in region (2), RHEED intensity increased initially since the surface was a little As-rich, and then decreased, similar to the onset of MBE growth. Figure 13 shows the effect of As_4 pressure on RHEED oscillations during MEE of InAs at a shuttering period of 1.47 second. While In and As_4 fluxes were deposited alternately, the As_4 pressure was reduced from ~ 8×10^{-6} torr to ~ 2×10^{-6} torr in ~ 90 seconds.With decreasing As_4 pressure the RHEED intensity increased first. This means that in the beginning, As_4 had an over pressure. When As_4 pressure decreased to a certain level, the RHEED intensity reached a maximum and the RHEED intensity oscillation curve looked the smoothest. This means that the As_4 pressure at this level was just right. After that, the oscillation intensity damps quickly because of shortage of As_4 resulting in damaged surface. A persistent RHEED oscillation was obtained for several hours under the optimized growth condition, as shown in Figure 14.

The quality of InAs epilayers on GaAs grown by MEE and MBE has been characterized with x-ray rocking curve analysis and Hall effect measurement. Figure 15 shows electron concentration as a function of growth temperature for unintentionally doped epilayers of about 0.6 μm thick grown by MEE and MBE, respectively. Under normal MBE growth conditions, InAs is grown under As_4 overpressure. Because of lower growth temperature compared with that of GaAs and much smaller atomic size ratio of arsenic over indium compared with that of arsenic over gallium, one can expect some extra arsenic atoms incorporated into the epilayer.

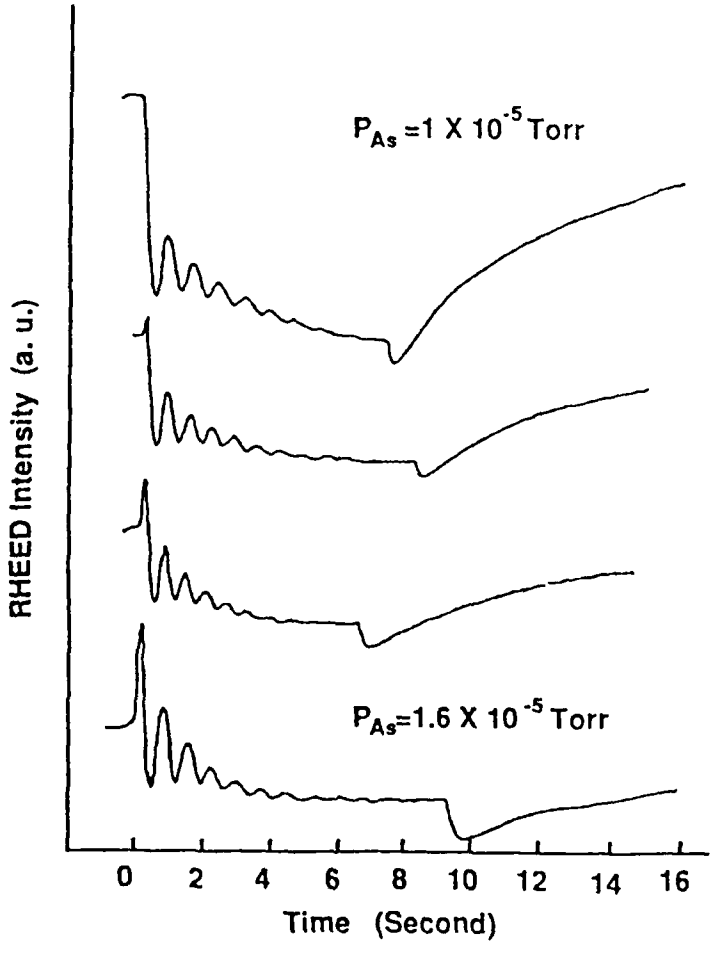

Figure 11 RHEED intensity oscillations during MBE of InAs at 500°C for different arsenic overpressures.

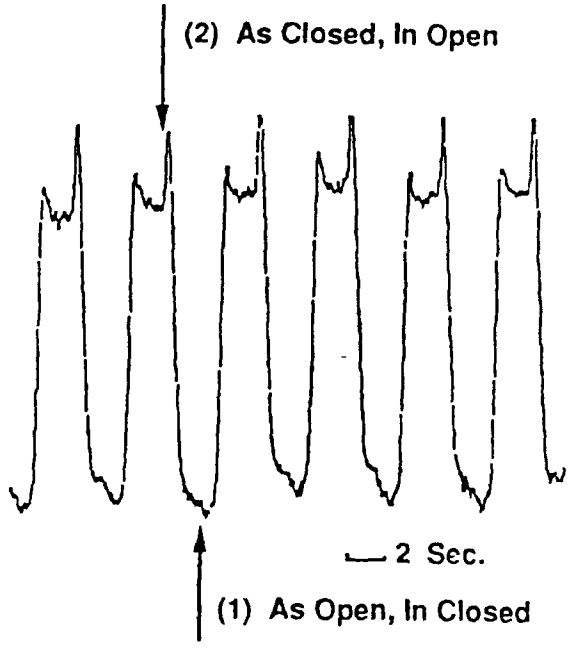

Figure 12. RHEED intensity modulation during MEE at arsenic overpressure (~ 6 x 10^{-6} to higher than optimal.

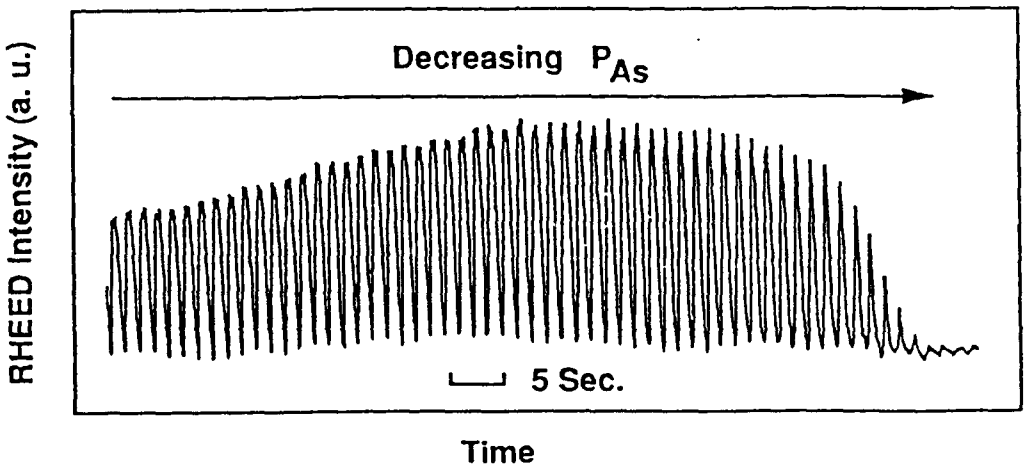

Figure 13 The effect of arsenic pressure (8×10^{-6} to 3×10^{-6} torr in ~ 90 seconds) on RHEED intensity oscillation during MEE.

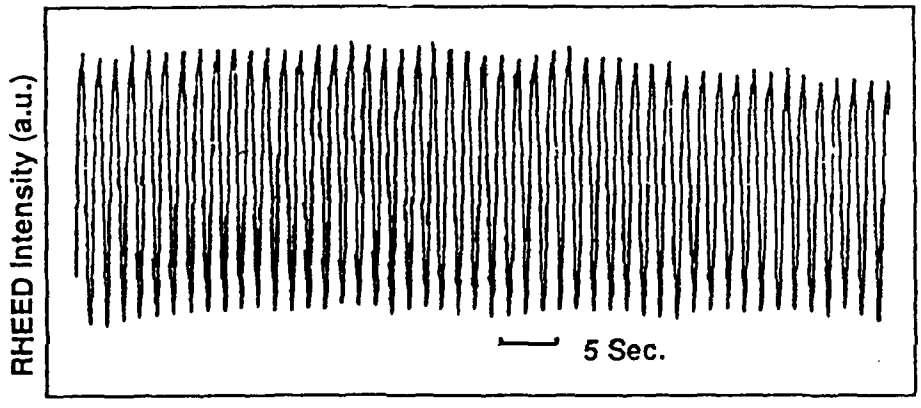

Figure 14 Persistent RHEED oscillations during MEE of InAs. Growth rate ≈ 0.37 μm/hr. $P_{As} \approx 4 \times 10^{-6}$ torr. Ts = 300°C.

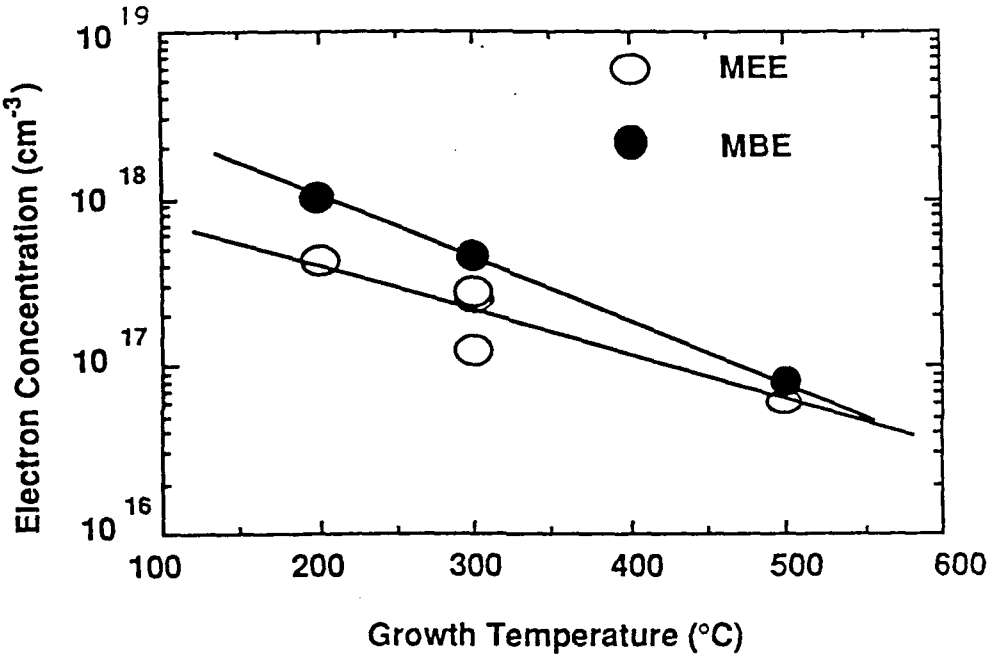

Figure 15 Electron concentrations in unintensionally doped InAs epilayers as a function of growth temperature for MEE and MBE (~0.6.μm thickness).

These arsenic atoms will occupy indium sites to produce antisite point defects. This kind of defect probably acts as donors in InAs. Thus, the lower the growth temperature, the higher the arsenic-rich related point defect concentration and the higher the electron concentration. However, because arsenic pressure was limited by optimized growth condition, much lower arsenic pressure was used in MEE than in MBE (5 times less). It is reasonable to expect that there will be lower arsenic-rich related point defect concentration in MEE than in MBE.

X-ray rocking curve analysis revealed 0.18 degree full widths at half maximum (FWHM) for a 1.4 micrometer-thick InAs epilayer grown by MEE at about 300°C but 0.20 and 0.5 degree FWHM for 3.0 μm and 0.74 μm InAs epilayer, respectively, grown by MBE at the same temperature and growth rate of 0.7 μm/hr. It is obvious that the quality of epilayers grown by MEE is better than that grown by MBE at low temperature.

2.3.3 Summary

Growth of InAs epilayers on GaAs (001) by MEE and MBE has been studied with RHEED. The effect of arsenic pressure on MEE RHEED intensity behavior was studied and optimized persistent RHEED oscillations were obtained. Hall effect measurement and x-ray rocking curve analysis revealed that at low growth temperature, the quality of InAs epilayer grown by MEE is better than that grown by MBE at the same temperature. This result was then applied to the MODFET program, as detailed in the next section.

2.4 AlGaAs/InGaAs MODFETs with Channel Layers Grown by MEE

The MODFET structure is basically the same as our standard structure, shown in Figure 1. We used MBE to grow a sequence of layers to be used for MODFET's with $In_xGa_{1-x}As$ channels and x ranging from 0 to 0.4. For the channel layer with high InAs molar fraction we also used migration enhanced epitaxy (MEE) at low substrate temperature, which provides the possibility of growing this very lattice-mismatched system monolayer by monolayer. The reason for using a low growth temperature of 400°C is to prevent In re-evaporation and intermixing between In and Ga atoms near interfaces.[17] The sequential MEE timing of $(InAs)_2(GaAs)_2$ is shown in Figure 16 The subscripts refer to the number of monolayers intended. Because the substrate surface is a nearly exact (100) surface, one-monolayer-high interface fluctuation in MBE or MEE $(InAs)_1(GaAs)_1$ seems to result in a random alloy. On the other hand,

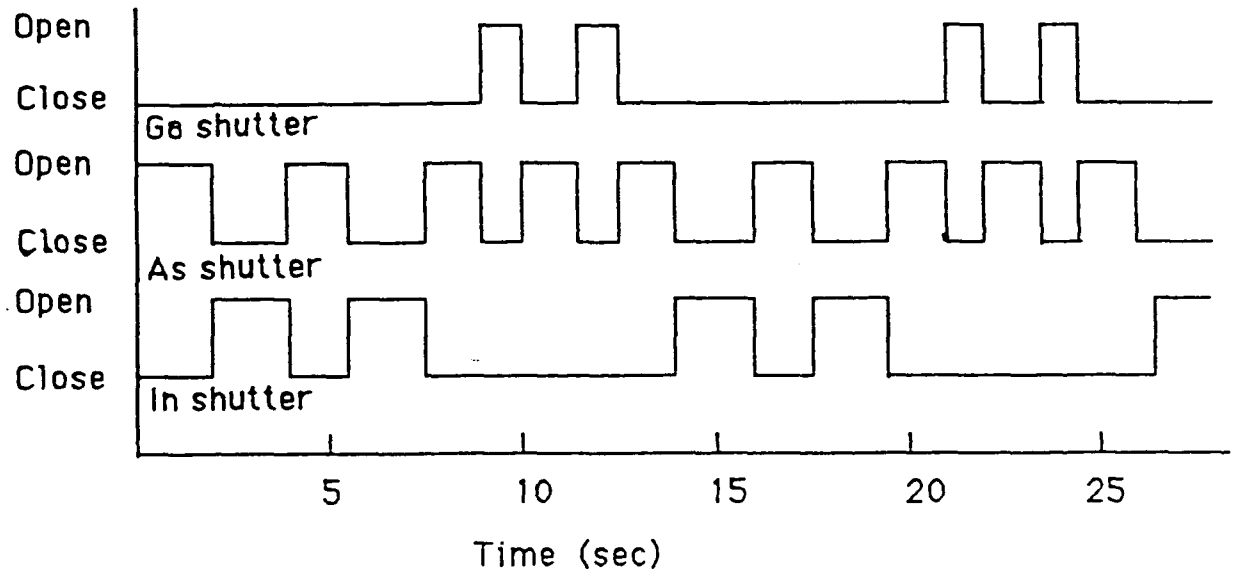

Figure 16 Sequential MEE growth timing of molecular beams.

there exists a large lattice mismatch (7.2%) between InAs and GaAs. Therefore, we limit the InAs and GaAs layers to be only two monolayers thick in MEE growth of active layers, to compare with MBE-grown random alloys. After the 20 Å GaAs spacer layer was grown to cap the channel layer, the substrate temperature was increased to 580°C to grow the AlGaAs spacer layer and the following layers.

2.4.1 Results and discussion

A. Transmission Electron Microscopy

Figure 17 shows a cross-section transmission electron micrograph (TEM) of the MODFET structure with a nominally $(InAs)_2(GaAs)_2$ channel. The channel layer shows nonuniform composition and undulating interfaces, probably because of considerable strain from the large lattice mismatch between InAs and GaAs. However, the interfaces are free of misfit-generated dislocations. There is some outdiffusion of In from the top region of the channel layer, as evidenced by less contrast in the top interface. We have tried to use Rutherford backscattering to estimate the In concentration. The results are inconclusive because of the nonuniform film thickness. Because the growth temperature of the nominally $(InAs)_2(GaAs)_2$ channel is low, we believe the average In composition to be close to 50%. The In concentration in the channel layer, however, still requires an independent determination.

B. Photoluminescence

Photoluminescence measurements at ≈ 40 K were performed in order to determine the quality of layers before device processing. Figure 18 shows PL spectra of samples with a random alloy $In_xGa_{1-x}As$ and a nominally $(InAs)_2(GaAs)_2$ channel. The peak at 830 nm is from GaAs epilayer. Another peak at longer wavelength is the channel subband transition peak which depends on the channel layer thickness, composition and strain relaxation. Figure 18a and 18b are spectra of samples with $In_{.17}Ga_{.83}As$ and $In_{.32}Ga_{.68}As$ channels, respectively. The peak from the $In_{.32}Ga_{.68}As$ sample is broader and weaker than the peak from the $In_{.17}Ga_{.83}As$ layer. As the In composition increases to 40% the 150 Å channel layer thickness exceeds the critical layer thickness. The strain relaxation in the channel layer generates misfit dislocations. No subband transition from the channel layer was observed because of poor crystalline quality as shown in Figure 18c. However, we

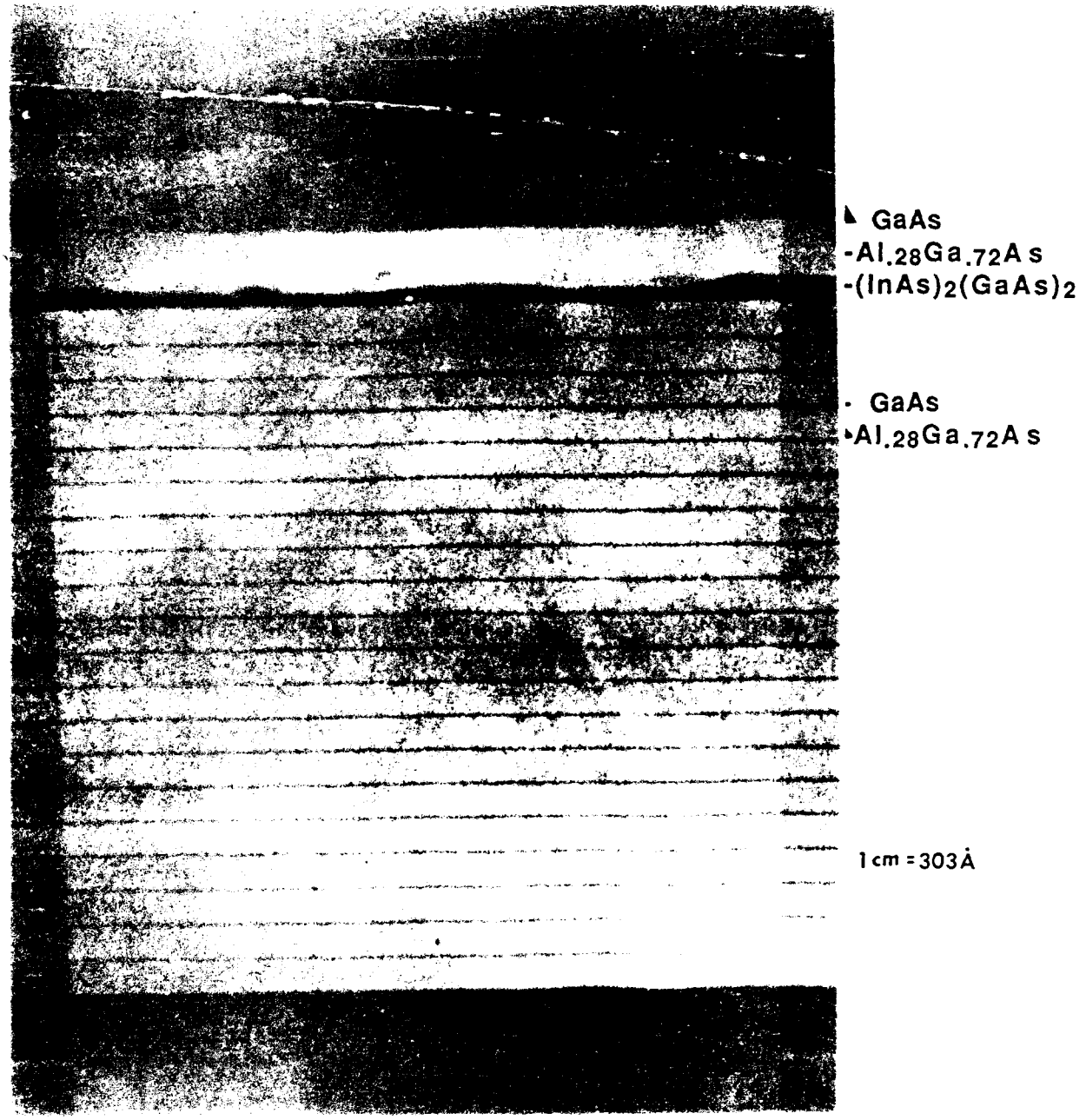

Figure 17 Cross-section TEM micrograph of the MODFET sample with a nominally $(InAs)_2(GaAs)_2$ channel. The magnification is 330,000.

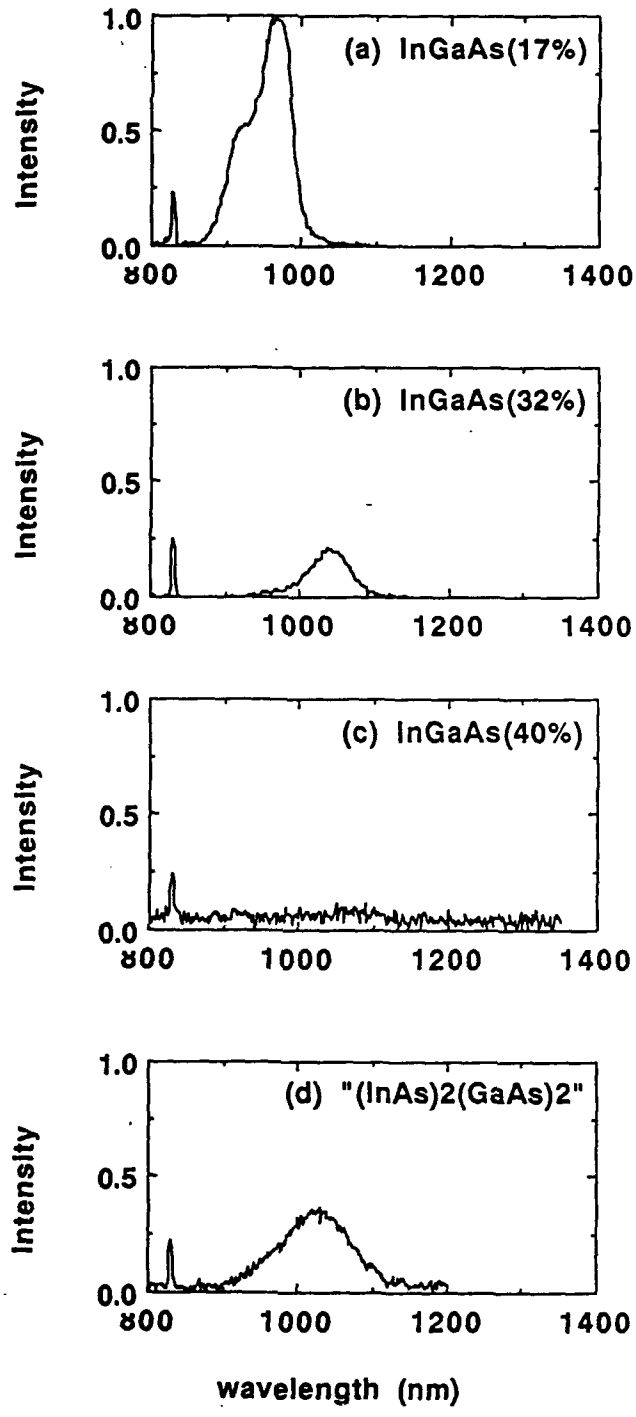

Figure 18 Photoluminescence spectra at ≈ 40 K. MODFET structure samples using random alloy $In_xGa_{1-x}As$ channel with (a) x = 0.17, (b) x = 0.32 and (c) x = 0.4. (d) MODFET structure samples using a nominally $(InAs)_2(GaAs)_2$ superlattice channel.

do observe a peak at about 1030nm from the nominally $(InAs)_2(GaAs)_2$ channel sample. Even though this peak is very broad and weak, It suggests that the nominally $(InAs)_2(GaAs)_2$ channel (150 Å thick) grown by MEE has a better crystalline quality than random alloy $In_{.40}Ga_{.60}As$ channel of the same thickness grown by MBE.

C. I-V characteristics

The device performances for samples with different In concentration in the channel are listed in Table 1.

TABLE 1
Transconductance g_m, drain saturation current I_{dss} measured at a gate voltage V_g of + 1.0 V, and unity power gain frequency f_{max} for MODFET with different In concentrations in the InGaAs channel layer.

In Concentration (%)	g_m (MS mm^{-1})	I_{dss} (mA mm^{-1})	f_{max} (GHz)
0	276	430	43
17	342	450	58
25	294	340	30
32	90	125	
40	40	50	
"$(InAs)_2GaAs)_2$"	130	200	

The MODFET sample with a random alloy $In_{.17}Ga_{.83}As$ channel showed a transconductance of 340 mS/mm and a saturation current of 450 mA/mm for a device with a 1μm gate length, 50μm gate width and 3μm source to drain spacing. The maximum frequency of oscillation was extrapolated to be 58 GHz. The I-V characteristics of the device is shown in Figure 19a, which also exhibited the low output conductance and excellent pinch-off. The breakdown voltage of this device is about 11-13 V. Figure 20 shows the transconductance and saturation drain current versus In composition of the channel layer. The lines between the data points are meant only to guide the eye. It is evident that the pseudomorphic InGaAs channel MODFET has better device performance than lattice-matched GaAs channel MODFET. On the other hand, as the In composition in the channel increases, the lattice mismatch exceeds the pseudomorphic growth range which results in significant degradation in device performance. In Figure 19b we show the I-V

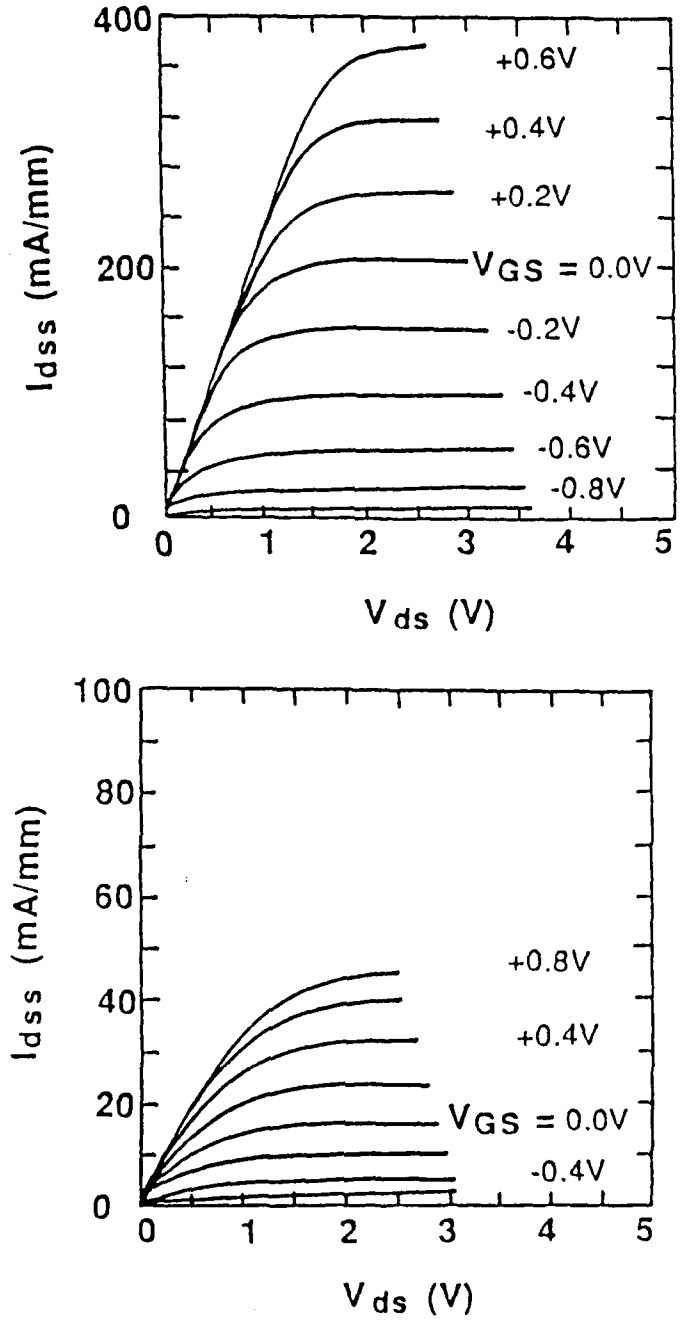

Figure 19 Drain current-voltage output characteristics for a MODFET with a random-alloy $In_xGa_{1-x}As$ channel. (a) x = 0.17 and (b) x = 0.40.

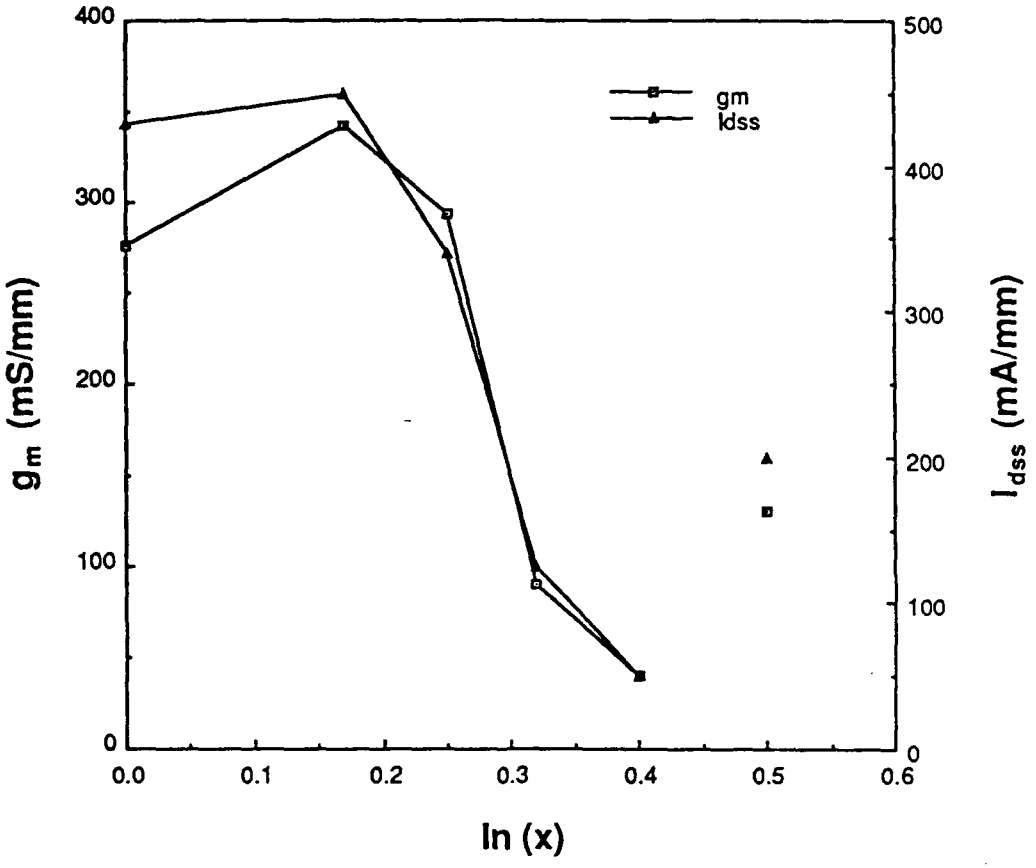

Figure 20 Transconductance and saturation current versus InAs molar fraction in the channel.

characteristics of the sample with $In_{.40}Ga_{.60}As$ channel for comparison. For the samples with $In_{.32}Ga_{.68}As$ and $In_{.40}Ga_{.60}As$ channels we could not make s-parameter measurements.

Of particular interest is the sample with a nominally $(InAs)_2(GaAs)_2$ superlattice channel, which shows reasonable transistor characteristics, i.e., a low output conductance, transconductance of 130 mS/mm and saturation current of 200 mA/mm. The drain I-V curves shown in Figure 21 are to be compared with Figure 19b. Although these results are not as good as those obtained from the $In_{.17}Ga_{.83}As$ sample, they are much better than those obtained from the $In_{.40}Ga_{.60}As$ sample.

2.4.2 Summary

We have investigated the luminescent and device properties of pseudomorphic AlGaAs/InGaAs modulation-doped field-effect transistors (MODFET's) with different InAs molar fractions in the InGaAs channel. We used MBE to grow the random-alloy $In_xGa_{1-x}As$ channels for x up to 0.4, and we used MEE to grow a nominally $(InAs)_2(GaAs)_2$ channel for an effective x of near 0.5. For 1-micron-gate-length MODFET's with random-alloy $In_xGa_{1-x}As$ channels the transconductance g_m and saturation drain current I_{dss} exhibit a maximum at $x = 0.17$, and decrease drastically for x higher than 0.32 because of misfit dislocation generation. The photoluminescence peaks of $In_xGa_{1-x}As$ channels of these MODFET samples show a similar trend; strong intensity for the $In_{0.17}Ga_{0.83}As$ channel and very weak intensity for the $In_{0.4}Ga_{0.6}As$ channel. However, MODFET's with a nominally $(InAs)_2(GaAs)_2$ channel grown by MEE exhibit higher g_m, I_{dss} and photoluminescence intensity than those with a random alloy $In_{0.4}Ga_{0.6}As$ channel grown by MBE. Cross-section TEM micrographs indicate some outdiffusion of In from the top interface of the nominally $(InAs)_2(GaAs)_2$ superlattice channel. Because the MEE-grown layer was grown at low temperature, we believe that the In concentration is still close to 0.5. In addition, in cross-section TEM few dislocations are observed at the MEE-channel/buffer interface. An independent determination of the effective In concentration is still required.

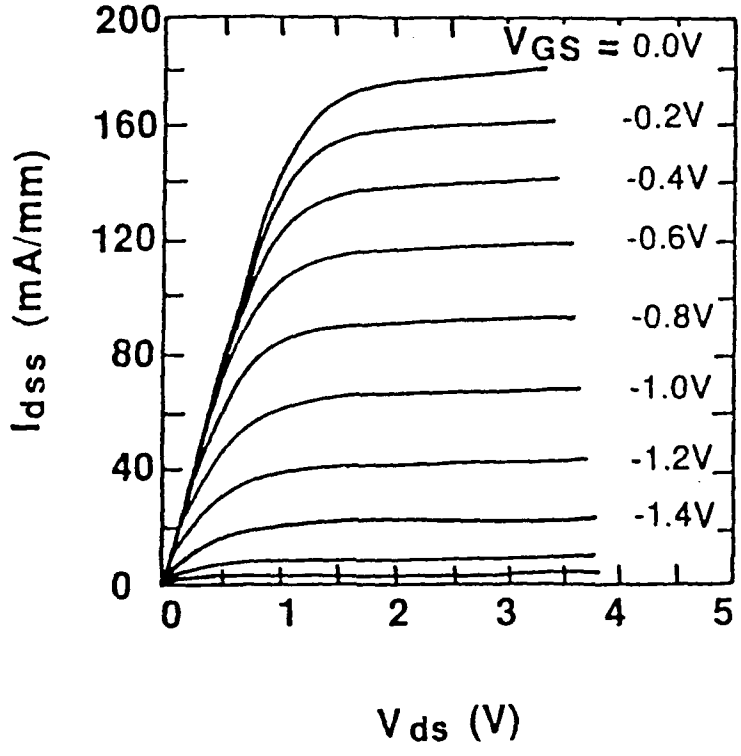

Figure 21 Current - voltage output characteristics for a MODFET with an $(InAs)_2(GaAs)_2$ superlattice channel, corresponding to InAs molar fraction of 50%, with transconductance of 120 mS/mm and saturation current of 200 mA/mm at Vg = 1.0 V.

3. InGaP/InGaAs MODFET Structures

3.1 Establishing a Gas-source MBE System

During this contract period, we have set up a gas-source MBE system with hyride/solid-source combination. Elemental group-III and thermally cracked arsine and phosphine sources are used. Figure 22 shows a schematic of the gas-handling system. We have collaborated with the Environmental Health and Safety Department at UCSD in installing the safety interlocks and toxic gas exhaust system. Separate gas cabinets are used to house 100% arsine and 100% phosphine cylinders. Exhaust from the cryopump goes through a glass column filled with potassium permanganate ($KMnO_4$), which, after oxidizing arsine and phosphine, changes color from pink to brown. Before changing the cylinders, the gas-manifold is purged by nitrogen. The purged residual gases are exhausted through another scrubber.

The GSMBE system consists of a modified Varian Modular GEN-II MBE reactor equipped with a 2200 l/s (H_2) cryopump and an ion pump (which is turned off during growth). As a result of large quantity of hydrogen from cracking arsine or phosphine, the cryopump has to be regenerated after about 2 days of use. However, we find that a gas source is so much easier to work with than a solid source arsenic because the flux can be controlled at will by simply changing mass-flow controller settings. In addition, source utilization is very efficient. It turns out that the amount of phosphine in the pigtail can last for several hours.

3.2 Optimizing Growth Conditions for Phosphides

Gas-source molecular-beam epitaxy is a viable technique for growing phosphides because it may provide more precise control of phosphorus flux than conventional molecular-beam epitaxy (MBE) and better layer thickness control than liquid-phase epitaxy or vapor-phase epitaxy.[18] Critical issues of high-quality epilayer growth are the growth temperature and V/III ratio. In conventional MBE, the V/III ratio is obtained by measuring beam equivalent pressure. In GSMBE the high hydrogen background pressure (typically 1×10^{-5} Torr) makes accurate V/III ratio measurement by ion gauge difficult. Another problem is that the V/III ratio at the substrate surface depends on the growth temperature, thus will be different from the beam flux ratio. Panish and Sumski demonstrated a calculation of the group-V beam flux at the substrate surface by converting the equilibrium group-V partial pressure in a solid+liquidus system for GaAs and InP in GSMBE.[19] Group-V-controlled growth rate measurement goes

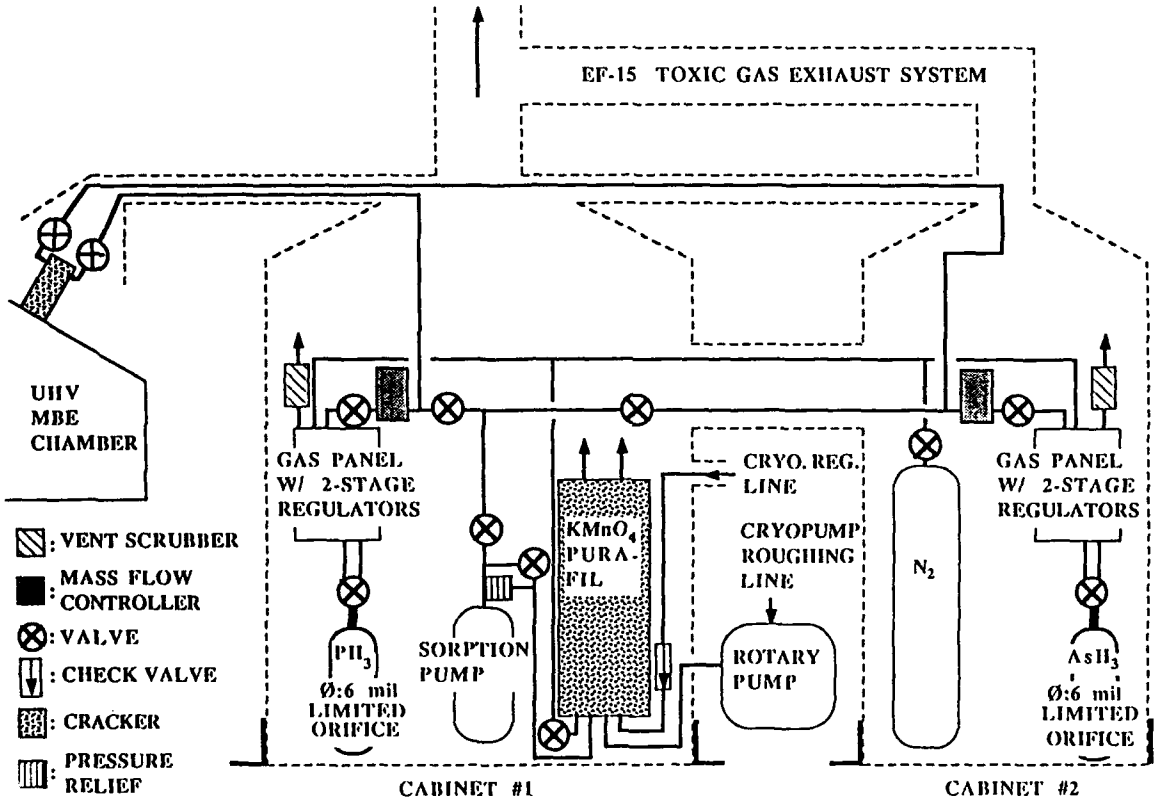

Figure 22 A schematic diagram of the gas-handling system for GSMBE.

even further by measuring the amount of group-V incorporated into the epilayer regardless the chamber geometry, ionization factor of the ion gauge and high hydrogen background pressure.[20,21] Similar experiment of arsenic-controlled growth rate measurement in conventional MBE has been used to measure the arsenic incorporation rate and sticking coefficients of both As_2 and As_4 on GaAs (100).[22] Here we report for the first time phosphorus-controlled growth rate measurement of InP, GaP and AlP in GSMBE.

3.2.1 Experimental procedures

Both arsine and phosphine are introduced into the growth chamber through the same Varian hydride injector. The normal cracking temperature is 1000°C. The phosphine flow rate in this study is typically 1-4 sccm. The background pressure ranges between 0.8×10^{-5} and 2×10^{-5} Torr during growth. The growth rates are monitored by the specular beam intensity oscillation of RHEED. A dual-channel differential amplifier[23] produces clean RHEED signals after subtracting the background noises. The oscillation is then recorded in an IBM PC AT compatible computer to measure the growth rate.

InP (100) substrates were degreased in a 1% Alconox solution and then rinsed with DI water. They were etched afterwards in a solution of H_2O_2:NH_2OH:H_2O (2:5:10), rinsed, and blown dry. For GaP (100), there is an additional step of 50% HCl dip before the final rinse. Each sample was bonded onto a 3-inch Si wafer with In. The Si wafer was then mounted onto a Mo transfer ring with Ta wires. Growth temperatures were calibrated with a pyrometer and the melting point of InSb.

3.2.2 Results and discussion

Figure 23(a) illustrates a typical RHEED oscillation and shutter operating sequence during the growth of GaP at 610°C. It started with a phosphorus-stabilized surface. Then Ga-induced oscillation was observed after the Ga shutter was opened. The RHEED intensity decreased after the phosphine shutter was closed because of the Ga accumulation on the substrate which formed a rough surface. The final step involved closing the Ga shutter and opening the phosphine shutter again. Here the oscillation resumed with incoming phosphorus species and previous Ga accumulated on the surface. This represents phosphorus-controlled growth because there was an excess amount of Ga atoms on the surface and the available amount of phosphorus limited the growth rate. While routinely taking data, we just deposited several layers of Ga on the surface without phosphine, then the closed Ga shutter and opened the

phosphine shutter at the same time. The resultant oscillation is shown in Figure 23(b). The same experiments were performed in growing InP at 470°C and AlP at 615°C. Figure 24 shows the growth rates of (a) GaP, (b) AlP, and (c) InP as a function of the reciprocal group-III cell temperatures. The phosphorus-controlled growth rates, as measured by the procedures just mentioned, are shown with thick lines. They are independent of group-III fluxes.

For the case of InP, a different approach was also used to obtain phosphorus-controlled growth. With phosphine flow rate fixed the In-controlled growth rate was measured under various In fluxes. As the open circles show in Figure 24(c), the natural logarithm of the growth rate increases linearly with the reciprocal In cell temperature. This linear dependence stops at certain points then the growth rate become constant as In flux increases more. These points at which the growth rate saturates indicates unity V/III ratios, that is, In-controlled growth rate equals P-controlled growth rate. Growth rate in the plateau region is controlled by the phosphine flow rate, independent of the In flux. Figure 25(a) and (b) show RHEED oscillations of InP using different In fluxes. Both oscillations were taken under indium-rich conditions. At time t_1 the In shutter was opened. Since the V/III ratio was less than unity in this region, the excess In atoms were accumulated on the surface so that the growth continued even when the In shutter was closed at t_2. The V/III ratio in Figure 25(b) was even smaller than that in Figure 25(a). This results in more oscillations after t_2 in Figure 25(b) than that in Figure 25(a). One important feature of these oscillations is that the growth rate between t_1 and t_2 is the same as the growth rate after t_2. This identifies phosphorus-limited growth and the growth rate in this region depends only on the phosphine flow rate. Figure 26 combines the data from InP, GaP, and AlP. It shows linear behavior of phosphorus-limited growth rate versus phosphine flow rate in GSMBE. This demonstrates the precise flux control capability of GSMBE. The slope will strongly depend on growth temperature. Here the same slope shared by the three different materials suggests that the P_2 incorporation coefficients in InP, GaP and AlP are equal under growth temperatures used in this study.

From the results in Figure 23 and Figure 25, we can obtain an accurate measure of the V/III ratio while growing all phosphides. For a given group-III flux and V/III ratio, we can set the corresponding phosphine flow rate accurately. An InP layer with 77K mobility 62,600 cm^2/V-sec and background donor carrier concentration of 5. 1 x 10^{14} cm^{-3} was achieved under V/III≈1 condition. Electrical and optical

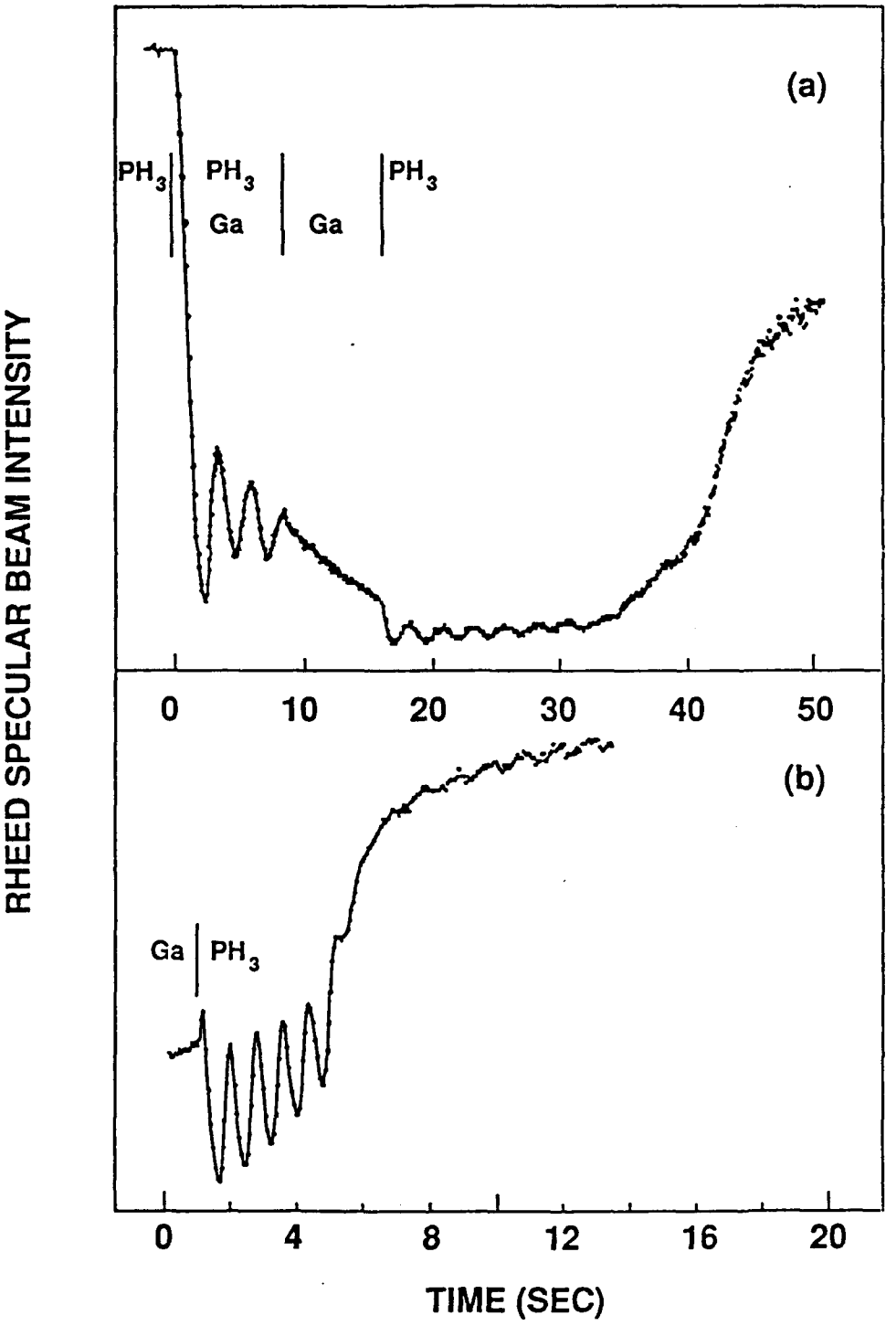

Figure 23 (a) RHEED oscillations of Ga-and phosphorus-induced growth on GaP(100). The intensity decreases when Ga is deposited. (b) Typical phosphorus-induced RHEED oscillations. The intensity recovers after Ga is consumed.

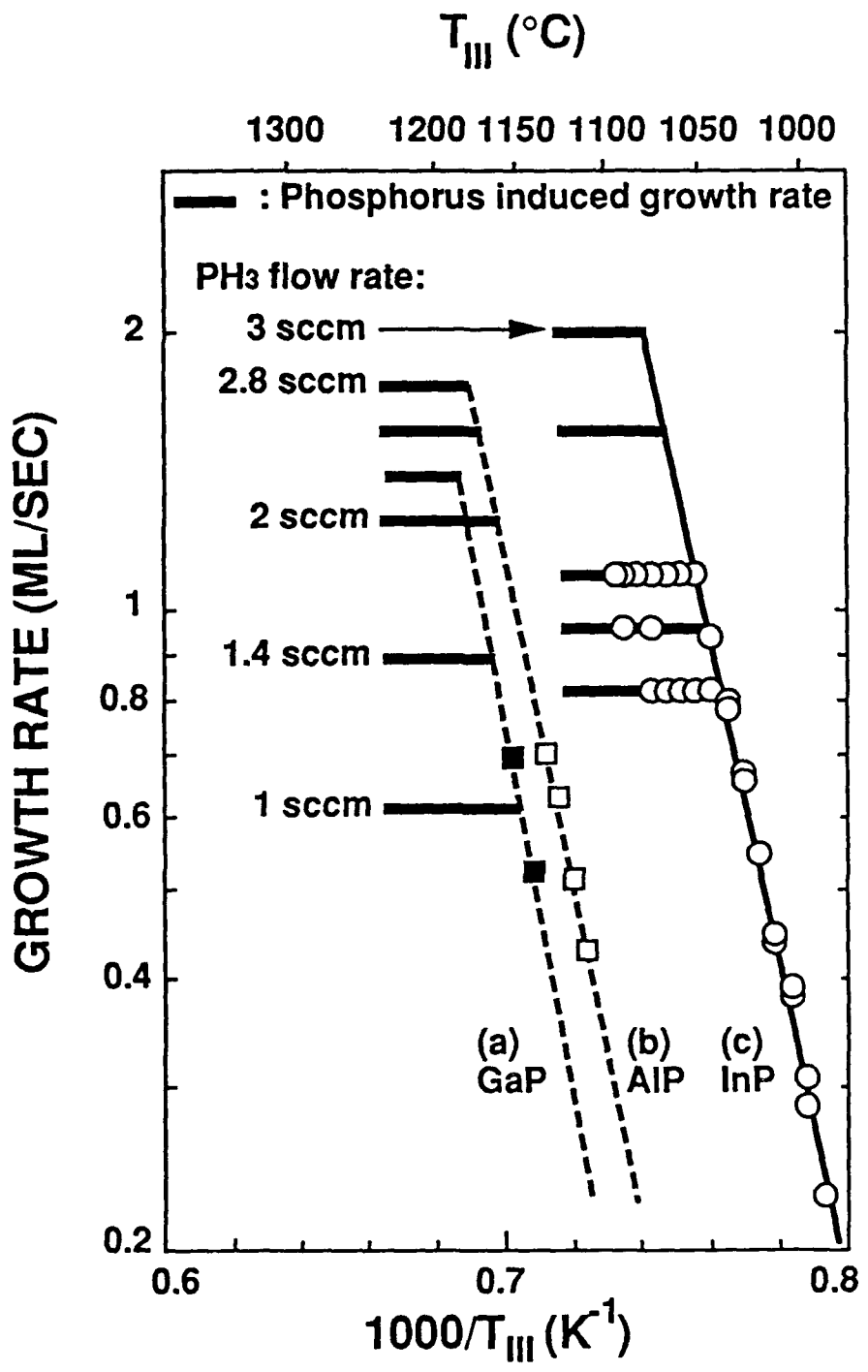

Figure 24 Growth rate versus reciprocal group-III cell temperatures for (a) GaP, (b) AlP, and (c)

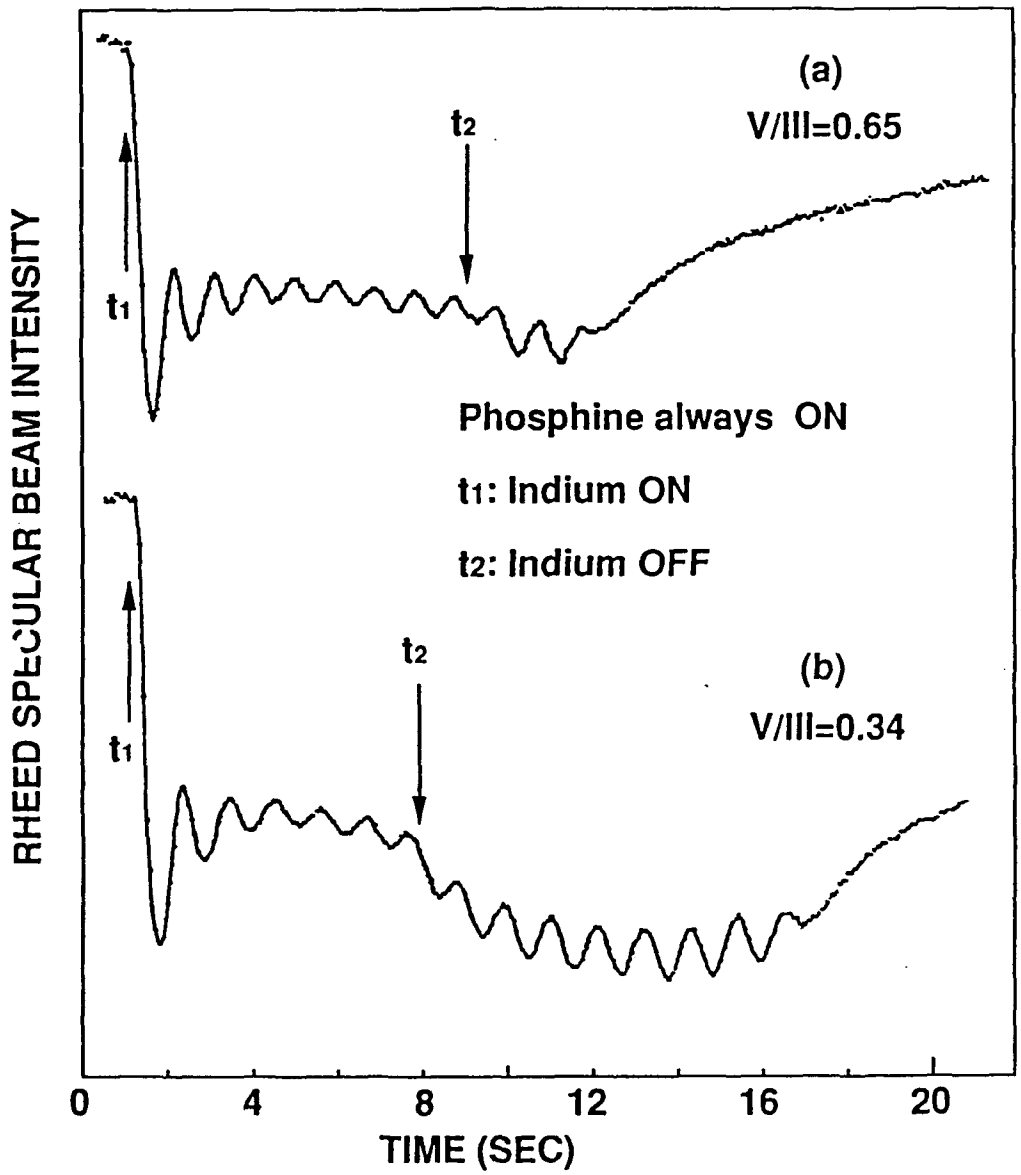

Figure 25 RHEED oscillations on InP (100) for $V/III_b < V/III_a < 1$. Notice the growth continues after the In shutter is closed at t_2 owing to accumulated In on the surface.

properties of epilayers grown under different V/III ratios are currently under investigations. Preliminary study of growth of arsenides by arsine in GSMBE yields similar results. Accurate V/III ratio control is very important for composition control in growing compounds containing mixed group-V elements, e.g., $GaAs_xP_{1-x}$ and $In_yGa_{1-y}As_xP_{1-x}$. The value of *x* in these compounds is not easily determined by the flow rate or the beam flux measured by an ion gauge. Combining the results of both phosphine and arsine will provide a convenient and precise way to control the *x* value in mixed-group-V compounds.[24]

The substrate temperature (Ts) dependence of phosphorus-controlled growth was also investigated on GaP and InP[25]. The results are shown in Figure 26. On InP, the growth rate starts to decrease for Ts ≥ 440°C. The P_2 surface desorption activation energy is estimated to be 0.82 eV. For GaP the phosphorus-controlled growth rate is fairly constant at substrate temperature from 550°C to 650°C and then decreases for Ts > 650°C owing to phosphorus desorption. The activation energy is measured to be in the range of 0.89-0.97 eV on the Arrhenius plot. These values are much larger compared to the As_2 incorporation activation energy obtained by Chow and Fernandez,[22] which were measured to be 0.2 eV on GaAs with similar experiments in conventional MBE.

3.2.3 Summary

In conclusion, the phosphorus-controlled growth of InP, GaP and AlP by GSMBE was determined experimentally. Growth rates were measured under different group-III fluxes, phosphine flow rates, and substrate temperatures. This technique, which measures the amount of phosphorus actually being incorporated in the epilayer growth can achieves precise control of V/III ratio. Phosphorus surface desorption activation energies are also measured for GaP and InP.

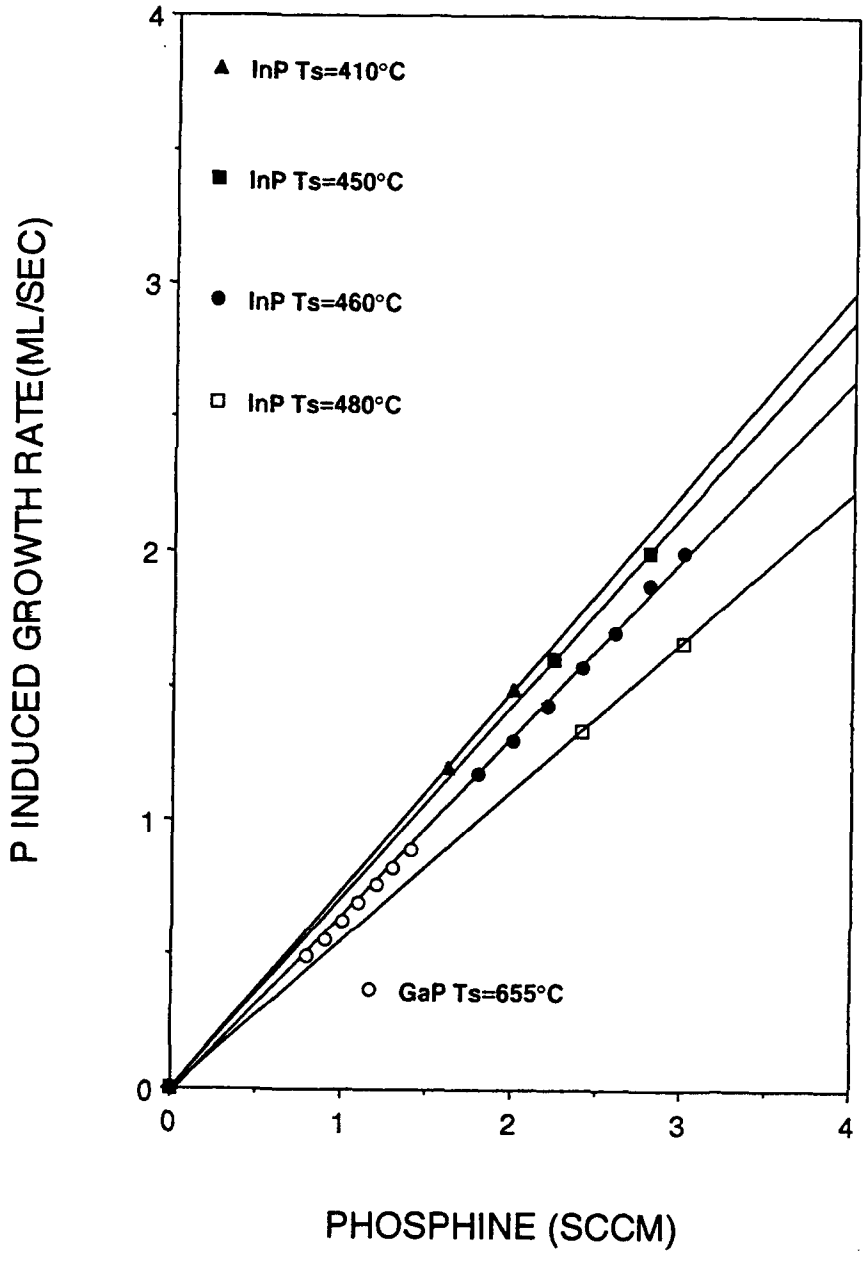

Figure 26 Group-V-induced growth rate versus the hydride flow rate.

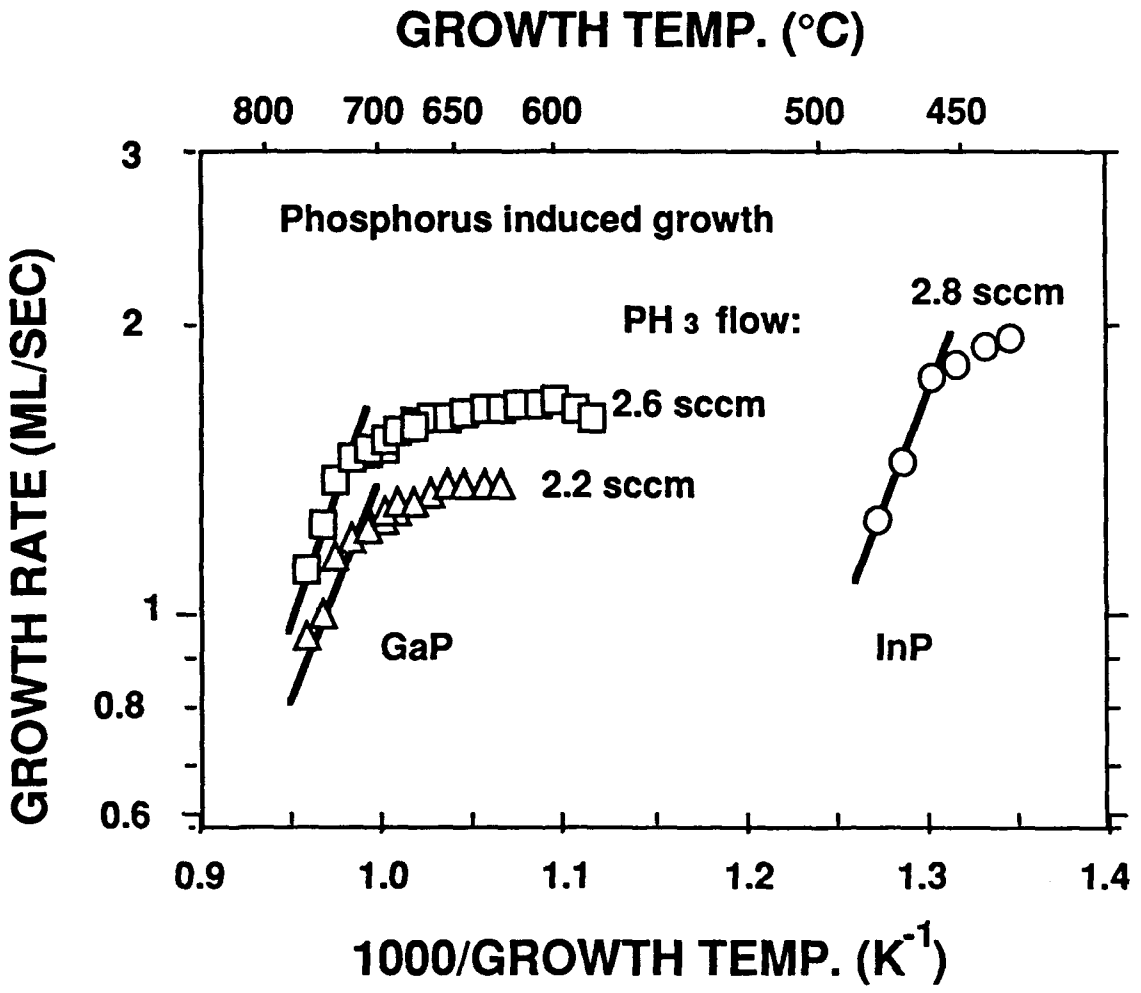

Figure 27 Arrhenius plot of phosphorus-induced growth rate versus substrate temperature.

3.3 Interface Properties Involving Arsenic and Phosphorus

In this section we present high-resolution x-ray diffraction (HRXRD) data from InAlAs/InP superlattices grown by gas-source molecular-beam epitaxy (GSMBE) on (001) InP. Narrow peak widths and clear Pendellosung oscillations are observed, indicative of very high quality material both in lateral uniformity and periodicity. We also quantify from theoretical simulations of the data based on dynamical diffraction theory the intermixing which occurs at each interface. Such intermixing is to be expected from this system since the growth requires that the group V elements, As and P, be switched at each heterointerface. Compositional intermixing and localized strain have been detected by HRXRD and other techniques at similar heterointerfaces including InGaAs(P)/InP[26,27]superlattices, InGaP/GaAs[28,29] multiple quantum wells and AlInP/GaAs[30] single quantum wells. In this work we quantify the composition and thickness of the interfacial layers occurring at InAlAs/InP superlattices. Simulations of (004), (002), and (115) x-ray rocking curves with excellent fits to the data are obtained if one monolayer thick strained intermixed layers are included in the superlattice structure.

3.3.1 Experimental procedures

The shutter/valve sequence for growing superlattices and the nominal structure are shown in Figure 28 (a). The growth temperature of the structure was 520°C. The 4-second hydride (arsine or phosphine) flow before growing each new layer was implemented to stabilize the gas flow while switching the hydrides.

X-ray rocking curves were recorded using a diffractometer with a four-reflection monochromator consisting of two channel-cut germanium crystals (220 reflections), as first proposed by DuMond[31] and later described by Bartels[32]. This arrangement provides a very clean, symmetric beam profile with a full width at the half maximum (FWHM) of 12 arcsec. Cu $K\alpha_1$ radiation (λ = 1.54056 Å) was used for all reflections. Data were taken in 6 arcsec intervals with a 20-second counting time per point.

Simulations were performed with a PC386 computer using dynamical x-ray diffraction theory based on the solution of the Takagi-Taupin equations.[33] In the simulation, we consider each sample to be subdivided into layers of constant lattice parameter (*i.e.*, constant strain) and structure factor. The effect of the four-reflection monochromator in a (+,-,-,+) orientation was included in the calculation that follows the procedures described by Tanner[34] and Slusky and Macrander,[35] which ignores the effects of vertical divergence of the beam. Only reflecting power from the s

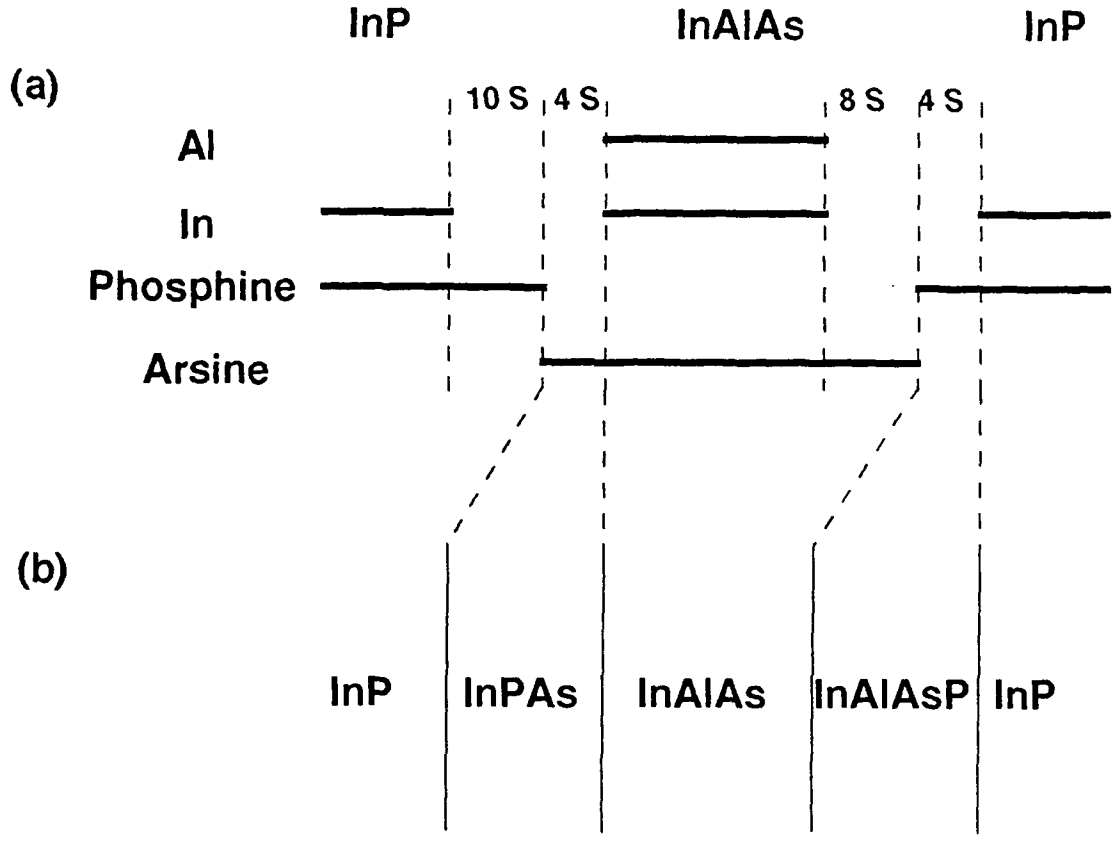

Figure 28 (a) Shutter and valve sequences for the growth of InAlAs/InP superlattices. The solid lines indicate when beams are on. There is a 4 s interruption while arsine and phosphine flows are switched. (b) The four-layer model including strained interfacial layers formed by As-P exchange.

polarization was simulated since the monochromator effectively blocks the π-polarized radiation.[35] The FWHM of our simulated rocking curve of the four-reflection monochromator was 12 arcsec, exactly the same as calculated by Bartels.[31] This curve was then correlated with the reflectivity curve of the sample crystal to give the final rocking curve. Peak broadening that is due to sample curvature was simulated by convoluting a rectangle of width 10 arcsec with the intensities derived from a flat sample.

3.3.2 Results and discussion

Figure 29 shows the (004) scan of a 20-period 80 Å $In_xAl_{1-x}As$/80 Å InP superlattice with a nominal composition $x = 0.52$ grown on (001) InP. Sharp and well defined satellite peaks could be detected up to order n = −5. The FWHM's of the experimental and simulated (without curvature) zeroth-order satellite peak are 50 arcsec and 48 arcsec, respectively. Such comparable FWHM's indicate that the superlattice crystal quality is nearly perfect. Pendellosung oscillations, clearly seen in the wings of the substrate peak, zeroth-order peak, +1 and −1 peaks suggest high crystal quality and perfection in the epilayer surface and interface. The superlattice period,[36] obtained from the averaged angular spacing between satellite peaks (1202 arcsec), was calculated to be 155 Å. The fact that the highest intensity peak within the envelope of superlattice reflections appears at a larger Bragg angle than the substrate implies the material is negatively strained, instead of perfectly lattice-matched. The averaged perpendicular x-ray strain[36] $\langle e_\perp \rangle$ (= $\langle \Delta a_\perp / a_{InP} \rangle$) of the superlattice, calculated from the angular separation between the main (n = 0) superlattice and the substrate peak, is -0.43%. If we assume that InP and $In_xAl_{1-x}As$ layers have equal thicknesses and that the InP layer is strain free (it is the same material as the substrate), $\langle e_\perp \rangle$ equals half the strain of the $In_xAl_{1-x}As$ layers (with no plastic relaxation). With a correction for tetragonal distortion[37] and application of Vegard's law, the In composition was calculated to be 0.49. From the period (60 arcsec) of the Pendellosung oscillations,[36] the number of periods in the superlattices was verified to be equal to 20.

The simulated rocking curve shown in Figure 29 (b) was obtained if we assume a perfect 20-period structure with abrupt interfaces, *i.e.*, a bi-layer model with layer thicknesses 78 Å for both InP and $In_xAl_{1-x}As$ layers and $x = 0.49$. This model resulted in a poor fit to the relative peak intensities of the superlattice peaks to the substrate peak, although it fit the peak positions very well. Since no physically viable

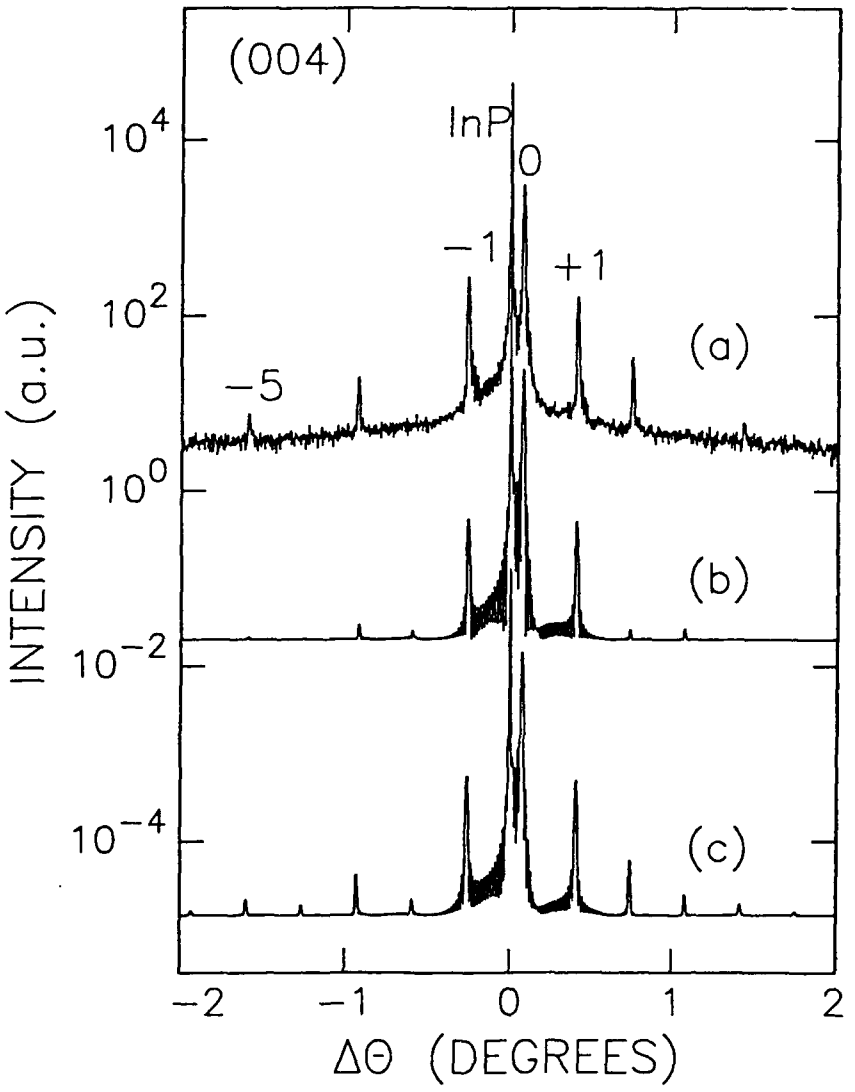

Figure 29 Experimental (a) and simulated (004) x-ray rocking curves of a 20-period superlattice consisting of (b) 78 Å $In_{0.48}Al_{0.52}As$ / 78 Å InP (abrupt interface) or (c) 76Å $In_{0.477}Al_{0.523}As$/3Å $In_{0.477}Al_{0.523}As_{0.95}P_{0.05}$ / 73 Å InP/3Å $InP_{0.40}As_{0.60}$ (4-layer model).

combination of layer thicknesses and In compositions could make the |n| > 1 satellite peaks increase in intensity by one order of magnitude, we, therefore, decided that the bi-layer model must be modified by the addition of a strained layer at each interface. This four-layer model, shown in Figure 28 (b), considered the top several monolayers of each InP layer to have some mixture of As and formed $InP_{1-x}As_x$ at the InAlAs-on-InP interface, while the top several monolayers of $In_zAl_{1-z}As$ were replaced by a quaternary compound $In_zAl_{1-z}As_{-1-y}P_y$ at the InP-on-InAlAs interface. The simulation program developed for this study allowed input compositions x, y, z and thickness for each layer to be varied. The period and averaged strain were kept constant, since the $InP_{1-x}As_x$ layer gave a positive strain and the quarternary layer contributed an additional negative strain. Figure 29 (c) shows a simulation with the best fit obtained with a four-layer model consisting of 73 Å of InP, 3 Å of $InP_{0.40}As_{0.60}$, 76 Å of $In_{0.477}Al_{0.523}As$, and 3 Å of $In_{0.477}Al_{0.523}As_{0.95}P_{0.05}$. This fit is excellent both in the shape of the superlattice envelope function and the intensities of the superlattice reflection relative to the substrate peak. Better fits to the experimental rocking curves could not be obtained either by choosing different lattice-parameter thickness profiles or by using 2 to 3 monolayers of interdiffused material. A three-layer model with only one intermixed layer at either the InAlAs-on-InP or InP-on-InAlAs interface also was not useful. Over 500 simulations of systematically chosen layer structures revealed that the intensity of the satellite peaks were very sensitive to the composition of the interfacial region and layer thickness. We found that the $InP_{1-x}As_x$ layer with positive strain affected the intensity of the n < 0 satellite peaks , while the InAlAsP layer with negative strain was crucial for the intensities of the n > 0 satellite peaks.

To support the validity of this four-layer model,[38,39] (002) rocking curves were also recorded and calculated using the best fit structure obtained from the (004) simulation. Although the (002) reflection is less suitable for calculation of strain, the satellite peaks are much stronger compared to those of the (004) reflections. Hence, the (002) reflection is more sensitive to superlattice properties. As shown in Figure 30(a), sharp and well defined satellite peaks could be seen up to n=+7 in the (002) experimental data. Excellent agreement between the simulated curve, shown in Figure 30(b), and the experimental (002) curve clearly shows the self-consistency of this model.

Symmetric reflections are sensitive to perpendicular strain only, while asymmetric reflections measure both perpendicular and parallel strains[39]. To investigate the coherency of the strained layers, the (115) reflection was measured and the result is shown in Figure 31(a). Figure 31(b) was calculated using the best fit parameters

from the (004) simulation with a parallel x-ray strain[40] (with respect to the substrate lattice constant) $e_{//}$ equal to zero. The excellent fit again adds further support to the self-consistency of the 4-layer model and confirms that plastic relaxation had not occurred.

The best structure determined by x-ray rocking curve simulations indicates that one monolayer of $InP_{0.40}As_{0.60}$ formed before InAlAs is grown and one monolayer of $InAlAs_{0.95}P_{0.05}$ formed on top of the InAlAs layer. We conclude that during growth 60% of the phosphorus on the top monolayer of InP was replaced by arsenic during the 4-second surface passivation by arsine. However, only 5% of arsenic in the top monolayer of InAlAs was exchanged by phosphorus within the same period of time. This is a reasonable result because of the low congruent evaporation temperature of InP (365°C). At the growth temperature of 520°C, the evaporation of phosphorus from InP and substitution of phosphorus vacancies by arsenic under arsenic overpressure is expected. Furthermore, owing to the higher melting temperature of AlAs (2013 K), InAlAs is expected to be stable at the growth temperature.

We have also considered the possibility of exchange or interdiffusion between In and Al occurring in addition to intermixing of As and P. This could form an unstrained InAlAsP (instead of InPAs) interfacial layer which would have the advantage of being thermodynamically stable. However, this model was ruled out by further simulations. Extra strain or large variations in structure factors from the interfacial region is necessary to produce the observed modulation in the satellite peak intensities. If the interface layers are unstrained the structure factor difference becomes the only factor. However, the magnitude of the structure factors of any of these layers is dominated by the In component, and hence they vary very little. Furthermore, simulations have shown that interfacial layers with strains of opposite sign at the two interfaces are necessary to make the intensities of odd satellites stronger than those of even ones,[41,42] as shown in our experimental curves. Thus, highly strained interfacial layers of opposite sign (in our case, InPAs layer with strain 0.37% and InAlAsP layer with strain –0.75%) must be formed to have the observed marked effect on the modulation of satellite peak intensities.

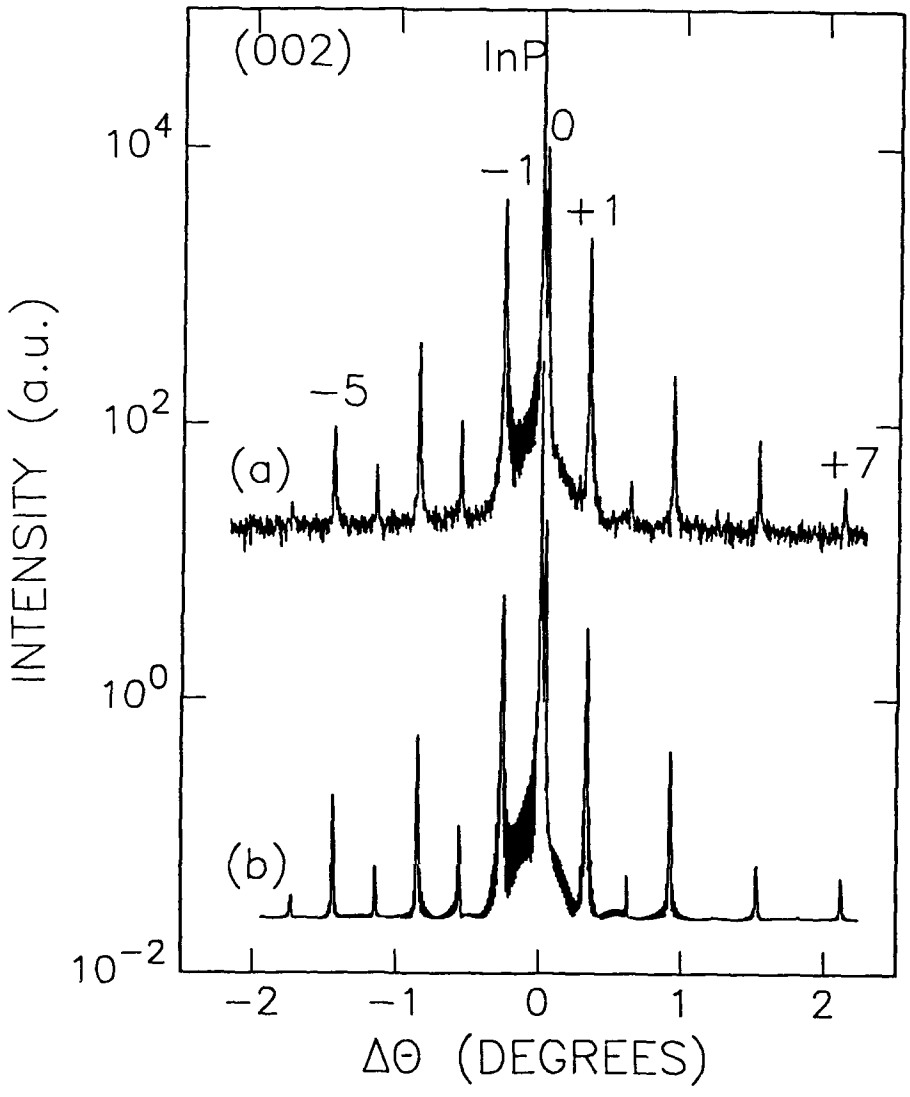

Figure 30 Experimental (a) and calculated (b) rocking curves for the (002) reflection from a 20-period superlattice assuming a four-layer model as in Fig. 28 (c).

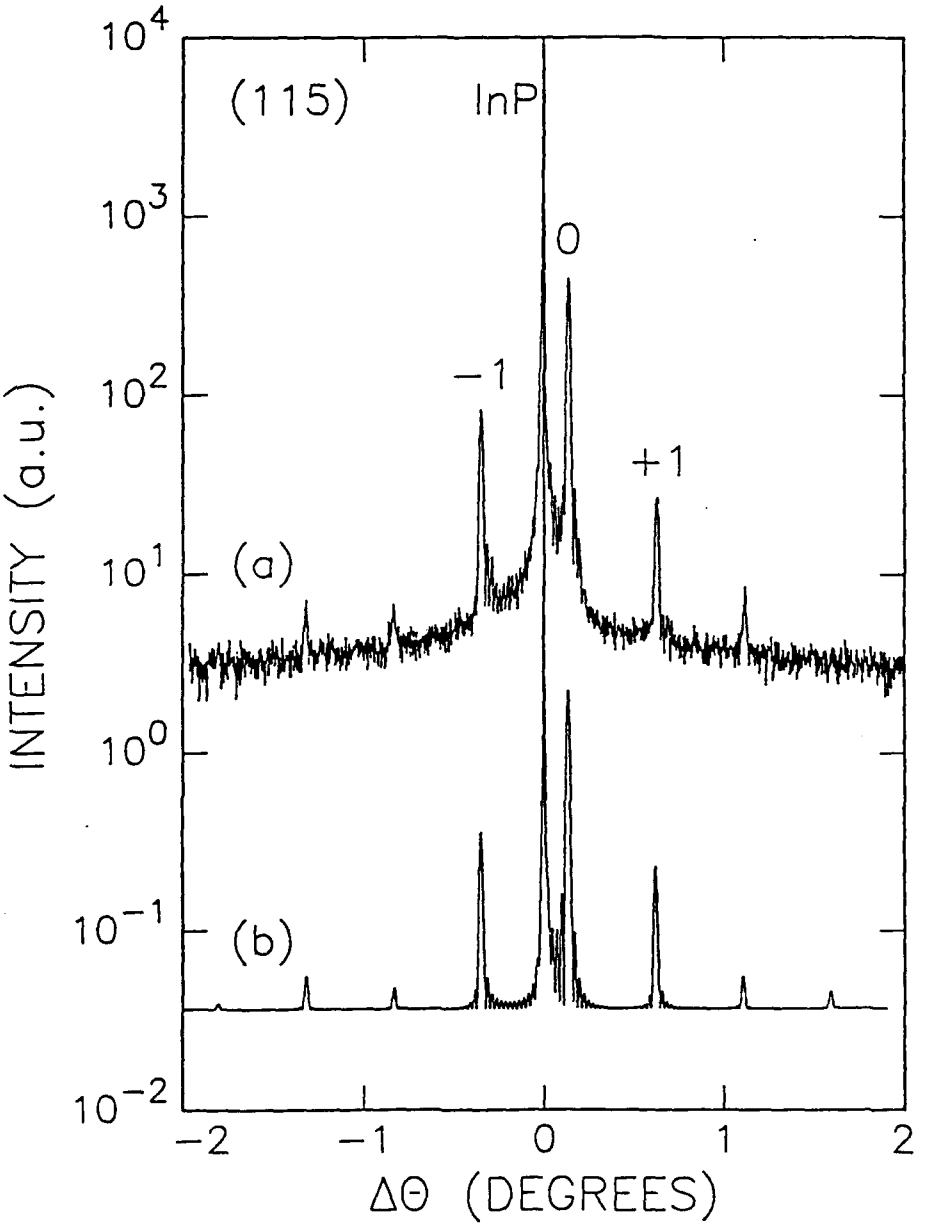

Figure 31 Experimental (a) and calculated (b) rocking curves for the (115) reflection from a 20-period superlattice assuming a four-layer model as in Fig. 28 (c).

3.3.3 Summary

In summary, we have used HRXRD to characterize the interface intermixing of As and P in InAlAs/InP superlattices. Excellent fits to (004), (002), and (115) rocking curves were obtained by simulations based on dynamical theory with the inclusion at each interface of a one-monolayer-thick strained intermixed layer. These simulations indicate that only As-P exchange occurs, and the composition of the interfacial layers are $InP_{0.40}As_{0.60}$ and $In_{0.477}Al_{0.523}As_{0.95}P_{0.05}$ at the InP and InAlAs surfaces, respectively.

3.4 InGaP/InGaAs MODFETs with an InAs/GaAs SL Channel

The advantages of using InGaP as a donor layer in an InGaP/InGaAs MODFET structure, as compared of using AlGaAs, are the absence of DX centers, which are due to Si and Al atoms, and the possibility of using a tensile-strained InGaP to compensate a compressive-strained InGaAs active layer.

We have grown such a structure, as shown in Figure 32.

$3x10^{18}$ cm^{-3}	GaAs	400 Å
$1x10^{18}$ cm^{-3}	$In_{0.5}Ga_{0.5}P$	300 Å
	$In_{0.25}Ga_{0.75}P$	105 Å
	$In_{0.25}Ga_{0.75}As$	105 Å
	GaAs	2000 Å
	Semi-insulating GaAs substrate	

Figure 32 A modulation-doped compensating-stress InGaP/InGaAs structure

After the doped cap layer was removed, the room-temperature mobility was 2,900 cm^2/Vs with a sheet carrier concentration of 7.9 x 10^{11} cm^{-3}, while the 77K mobility was 4,700 cm^2/Vs with a sheet carrier concentration of 6.6 x 10^{11} cm^{-3}. These results are very preliminary, indicating that more work is needed. Unfortunately, our Ga

furnace was out of order, and this project could not be continued. Many issues remain to be studied, besides optimizing the growth conditions. For example, the conduction band offset between $In_{0.25}Ga_{0.75}As$ and $In_{0.25}Ga_{0.75}P$ could be small because most of the bandgap difference could be in the valence band for a heterojunction between materials with different anions.

4. CONCLUSIONS

During the period September 30, 1988 and September 29, 1990, under contract #F33615-88-C-1861, we have investigated various approaches of compensating stress to increase the InAs molar fraction in an InGaAs-channel MODFET. Conventional solid-source MBE as well as hydride-source MBE were used. Because this contract represents the first ever for the PI and his students, the basic infrastructure of the laboratory and technology had to be established first. Key accomplishments included:

- Establishing a baseline AlGaAs/InGaAs pseudomorphic MODFET technology, with the best devices from 17% InAs molar fraction in the InGaAs channel. The maximum transconductance for such a device with 1 μm gate length is 342 mS/mm with a saturation current of 450 mA/mm (measured at a gate voltage of 1 V).
- Using an $(InAs)_2(GaAs)_2$ superlattice grown by migration-enhanced epitaxy at 400°C as the channel layer of a MODFET (with effective InAs molar fraction of 0.5) results in better luminescence properties and device performance than MBE-grown random-alloy $In_{0.4}Ga_{0.6}As$ as the channel layer.
- Setting up a gas-source MBE system with elemental group-III and doping sources and arsine and phosphine.
- Establishing precisely the V/III atomic ratio on the growing surface during gas-source MBE by using the RHEED oscillation technique in the group-V-limited growth mode.
- Understanding the As and P intermixing at interfaces in InAlAs/InP heterosturctures containing As and P in adjacent layers by high-resolution x-ray diffractometry and dynamic simulation of the x-ray rocking curves.
- Obtaining some preliminary results on modulation-doped, pseudomorphic InGaP/InGaAs structures.
- Producing 12 publications in referred journals and conference proceedings and 15 conference presentations on the above topics.

REFERENCES

1. For a review, see H. Morkoç and Unlu, *Semiconductor and Semimetals* **24**, 135 (1985).
2. J.N. Matthews and A.E. Blakeslee, *J. Cryst. Growth* **27**, 118 (1974).
3. R. People and J.C. Bean, *Appl. Phys. Lett.* **47**, 322 (1985).
4. P. Ribas, V. Krishnamoorthy, and R.M. Park, *Appl. Phys. Lett.* **57**, 1040 (1990).
5. E.F. Schubert, J.E. Cunningham, W.T. Tsang, and G.L. Timp, *Appl. Phys. Lett.* **51**, 1170 (1987).
6. C.T. Liu, S.Y. Lin, D.C. Tsui, H. Lee, and D. Ackley, *Appl. Phys. Lett.*, **53**, 2510(1988).
7. C. Guille, F. Houzay, J.M. Moison, and F. Barthe, *Surf. Sci.* **189-190**, 1041 (1987).
8. Y. Horikoshi, M. Kawashima, and H. Yamaguchi, *Jpn. J. Appl. Phys.* **27**, 169 (1988).
9. F. D. Schowengerdt, F. J. Grunthaner and John K. Liu, *Mat. Res. Soc. Symp. Proc.* **144**, 201 (1989).
10. B. W. Liang, K. Ha, J. Zhang, T. P. Chin and C. W. Tu, *SPIE Proc.* **1285**, 116 (1990).
11. R. Katsumi, H. Ohno, H. Ishii, K. Matsuzaki, Y. Akatsu, and H. Hasegagwa, *J. Vac. Sci. Technol. B* **6**, 593 (1988).
12. J.M. Gerard and J. Y. Marzin, *Appl. Phys. Lett.* **53**, 568 (1988).
13. H. Munekata, L.L. Chang, S.C. Wononick and Y.H. Kao, *J. Cryst. Growth* **81**, 237 (1987).
14. S. Kalem, *J. Appl. Phys.* **66**, 3097 (1989).
15. J.R. Soderstrom, D.H. Chow and T.C. McGill, *Mat. Res. Soc. Symp. Proc.* **145**, 409 (1989).
16. F.J. Grunthaner, M.Y. Yen, R. Fernandez, T.C. Lee, A. Madhukar, and B.F. Lewis, *Appl. Phys. Lett.* **46**, 983 (1985).
17. C. Guille, F. Houzay, J. M. Moison and F. Barthe, *Surf. Sci.* **189/190**, 1041 (1987).
18. M.B. Panish and H. Temkin, *Ann. Rev. Mat. Sci..***19**, 209 (1989)
19. M.B. Panish and S. Sumski, *J. Appl. Phys.* **55**, 3571 (1984).
20. B.F. Lewis and R. Fernandez, *J. Vac. Sci. Technol. B* **4** , 560 (1986).
21. R. Fernandez, *J. Vac. Sci. Technol. B* **6**, 745 (1988).
22. R. Chow and R. Fernandez, *Mat. Res. Soc. Symp. Proc.* **145**, 13 (1989).

23. C.E. Chang, T.P. Chin, and C.W. Tu, *Rev. of Sci. Instrum.* **62**, 655(1991).
24. H.Q. Hou, B.W. Liang, T.P. Chin, and C.W. Tu, unpublished.
25. T.P. Chin, B.W. Liang, H. Q. Hou, M.C. Ho, C.E. Chang and C.W. Tu, *Appl. Phys. Lett.*, **58,** 254 (1991).
26. J.M. Vandenberg, S.N.G. Chu, R.A. Hamm, M.B. Panish, and H. Tempkin, *Appl. Phys. Lett.* **49**, 1303 (1986).
27. J.M. Vandenberg, R.A. Hamm, M.B. Panish, and H. Temkin, *J. Appl. Phys.* **62**, 1278 (1987).
28. H.Y. Lee, M.J. Hafich, and G.Y. Robinson, *J. of Cryst. Growth* **105**, 244 (1990).
29. H.Y. Lee, M.J. Hafich, G.Y. Robinson, K. Mahalingam, and N. Otsuka, paper presented at the Sixth International Conference on Molecular Beam Epitaxy, La Jolla, California, August 27-31, 1990.
30. S. Nagao, M. Takashima, Y. Inoue, M. Katoh and H. Gotoh, paper presented at the Sixth International Conference on Molecular Beam Epitaxy, La Jolla, California, August 27-31, 1990.
31. J.W. M. DuMond, Phys. Rev. **52**, 872 (1937).
32. W.J. Bartels, J. Vac. Sci. Technol. B**1**, 338, (1983).
33. S. Bensoussan, C. Malgrange, M. Sauvage-Simkin, *J. Appl. Cryst.* **20**, 222 (1987).
34. B.K. Tanner, *Adv. x-ray Analysis* **33**, 1 (1990).
35. S.E.G. Slusky and A.T. Macrander, *J. Appl. Cryst.* **20**, 552 (1987).
36. B.M. Paine, *Mat. Res. Soc. Symp. Proc.* **69**, 39 (1986).
37. J. Hornstra and W.J. Bartels, *J. Cryst. Growth* **44**, 513 (1978).
38. M. H. Lyons and M.A. Halliwell, *Inst. Phys. Conf. Ser.* **76**, 445 (1985).
39. M. A. G. Halliwell and M.H. Lyons, paper presented at the Electrochemical Society Meeting, Montreal, Quebec, May 1990.
40. V.S. Speriosu, M.-A. Nicolet, S.T. Picraux and R.M. Biefield, *Appl. Phys. Lett.* **45**, 223 (1984).
41. C.R. Wie, H. M. Kim and K. M. Lau, *SPIE Proc.* **877**, 41 (1988).
42. E.G. Scott, M. H. Lyons, M. A. Z. Rejman-Greene and G.J. Davies, *J. Cryst. Growth* **105**, 249 (1990)

APPENDEX A

A. Some Results for p-channel Pseudomorphic MODFET's

As part of investigations on pseudomorphic structures, we have studied p-type doping by carbon using metalorganic molecular-beam epitaxy (MOMBE) and calculated the effects of strain on valence subband structures. In the course of experimenting with MOMBE of GaAs, we have studied the growth kinetics of MOMBE (see publications 1, 2, 4, and 5), possibility of atomic layer epitaxy (ALE) using trimethylgallium and arsenic (see publications 1 and 2), and a new kinetic model for the MOMBE process (see publications 3, 5, and 10). Because these topics are not directly applicable to the present contract, they are not included in this report. Paragraph A.1 describes the results on p-type doping, and paragraph A.2 summarizes a theoretical calculation on strained valence subband structures. The calculation was performed by Dr. Yan-Ten Lu and Prof. Lu Sham in the Physics Department, who were partially supported by the contract in the beginning.[A3]

A.1 p-type carbon doping by MOMBE

Similar to a number of reports,[A1] we obtained very high p-type doping by carbon, in the high 10^{19} cm^{-3} range for a growth rate of about 0.5 monolayers (ML) per second. The measurements were performed on a double ac Hall setup.[A2] Our data are shown in Figure A1, along with data obtained by the Aachen group.[A1] They obtained p-type doping from the 10^{14} to 10^{20} cm^{-3} range by using pure triethylgallium, trimethylgallium or a mixture of the two. Our sample results are 6.8X19 and 9.4X19 cm^{-3} with room temperature Hall mobilities of 92 and 78 cm^2/Vs, respectively. It is expected that the doping concentration would be higher for higher growth rate.

X-ray rocking curve measurement, taken with a four-crystal diffractometer, indicates the presence of strain that is due to heavy carbon doping and shows a small peak with a smaller lattice constant. This is as expected owing to the smaller size of the carbon atoms, compared to those of Ga and As. Figure A2 shows three x-ray rocking curves for (a) as-grown sample, (b) the same sample after furnace annealing at 400°C for 30 min., and (c) another peice after rapid thermal annealing (RTA) at 900°C for 10 sec. RTA was performed in a homemade setup under a flow of forming gas. The samples were placed under a piece of GaAs wafer and were first soaked at 550°C for 10 sec. Then the temperature was raised to 900°C in 5 to 8

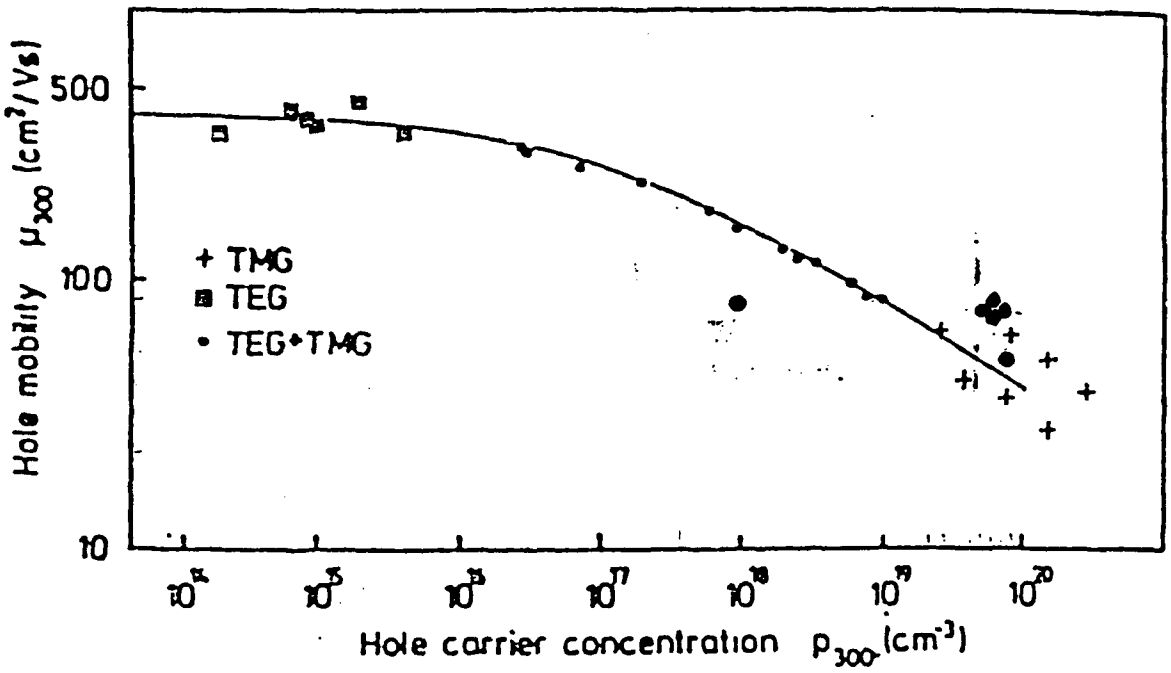

Figure A1 Room-temperature Hall mobility as a function of hole carrier concentration from the use of TMGa, TEGa, or their combinations. Our data are solid circles, and the other data points are taken from Ref. A1.

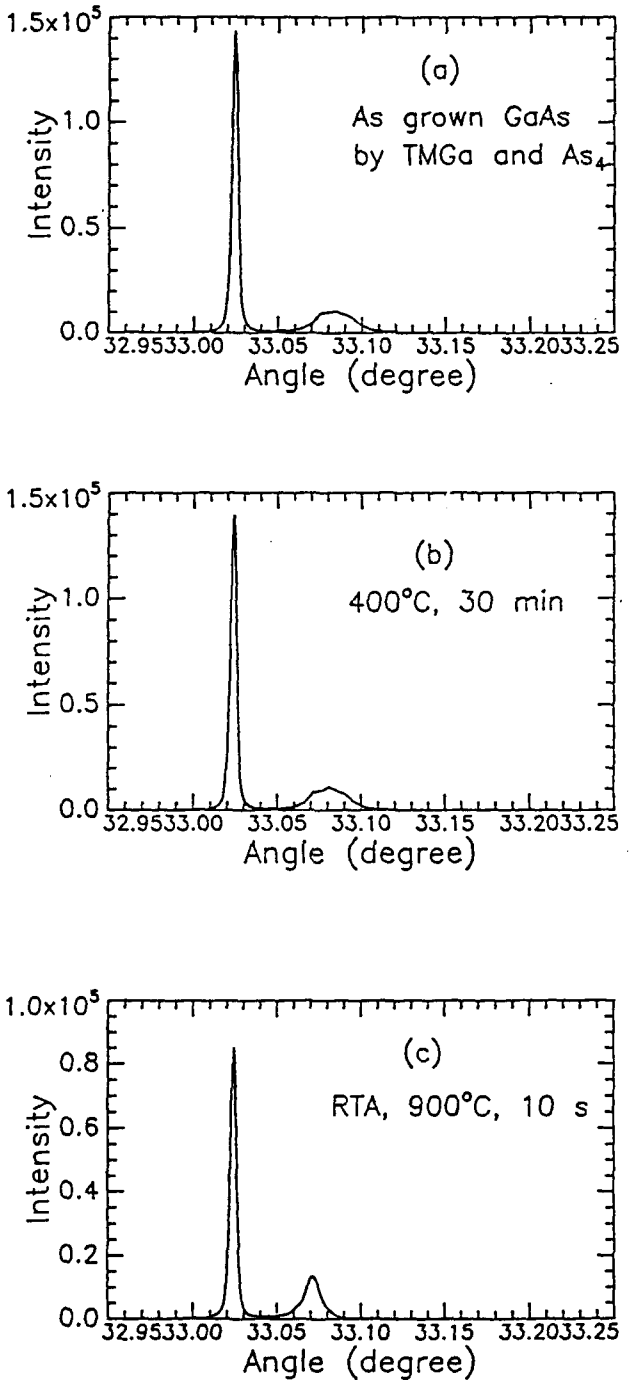

Figure A2 X-ray rocking curves of heavily carbon-doped GaAs for (a) as-grown sample, (b) the same sample after furnace annealing, and (c) another peice after RTA. The abscissa is rocking curve angles in degrees, and the ordinate is the x-ray intensity in an arbitrary unit. The sharp peak is due to the substrate, and the smaller and broader peak is due to the epitaxial layer.

sec. and stayed for 10 sec. Subsequently the power supply was turned off for rapid cool down.

It is clear that furnace annealing has no appreciable effect on the x-ray data but RTA improves the structural quality of the layer. The full width at maximum of the unannealed sample is ~ 90 arcsec, whereas that of the sample after RTA is ~ 45 arcsec. After RTA there is also a slight shift of the lattice constant towards that of GaAs. Hall measurement for a sample after RTA shows a small decrease in the carrier concentration, from 7.6×10^{19} to 6.8×10^{19} cm^{-3} with no change in the hole mobility (from 83 to 79 cm^2/Vs). The decrease in the free carrier concentration could be due to precipitate formation or site switching of the carbon atoms. Further study on the effect of RTA is required to elucidate this point. Nevertheless, RTA is a beneficial method for improving the crystalline structure without degrading electrical properties of the film.[A3]

A.2 Effects of strain on valence subband structures

Details of the calculations can be found in Dr. Yan-Ten Lu's Ph.D. thesis.[A4] Here we summarize his results. The structure of the valence band near the zone center was obtained by solving the 4 x 4 Lutthinger Hamiltonian,[A5] and the effect of strain was taken into consideration by the formulation of Bir and Pikus.[A6] The k.p model together with strain Hamiltonian embodies a correct description of the crystal symmetry, and therefore permits a meaningful study of the valence-band structure in the strained layer. Under biaxial (x and y) compression, the strain shift the center of gravity of the valence band to a lower energy, and split the degeneracy between the heavy-hole and light-hole subbands. The split heavy-hole band has higher energy than the split light-hole band, and possesses a lighter in-plane mass. In the Drude model, the mobility μ of a carrier is given by $\mu = e\tau/m^*$, where τ is the carrier relaxation time and m^* is its effective mass. If the highest valence band was light-hole-like over a sufficient energy range, then the hole mobility would be significantly enhanced, of benefit for p-channel and complementary logic applications.

For $In0_{0.20}Ga0_{0.80}As$ with lateral lattice spacing matched to the lattice constant of GaAs, the splitting between the heavy-hole and light-hole levels is about 100 meV. This large splitting greatly reduces the effect of the mixture between the heavy-hole and light-hole subband in the strained-layer AlGaAs/InGaAs/GaAs quantum well. The mixing of the heavy-hole and the light-hole subbands can thus be neglected in the calculation. The effect of doping, as in pseudomorphic MODFET's, was then studied using only the heavy-hole band. Within the Hartree approximation, the interaction between carriers was taken into consideration by the Poisson equation. The Schrodinger equation and Poisson equation were solved self-consistently. We have studied both the symmetric modulation-doped quantum well and the asymmetric modulation-doped quantum well. The effective field seen by a carrier in the symmetrically doped well is different from that in asymmetrically doped well, and therefore different responses to the gate voltate are expected for these two cases. In the asymmetrically doped quantum well, the separation of the acceptors and the carriers generates a dipole layer and incurs an internal potential jump in crossing the quantum well system.

Figure A3 plots the highest three confined levels and the effective potential for a symmetrically doped quantum well GaAs/InGaAs/GaAs. The modulation doping profile and the equilibrium charge distribution are plotted in Figure A4. The doped layers are located symmetrically on both sides of the quantum well, and each layer

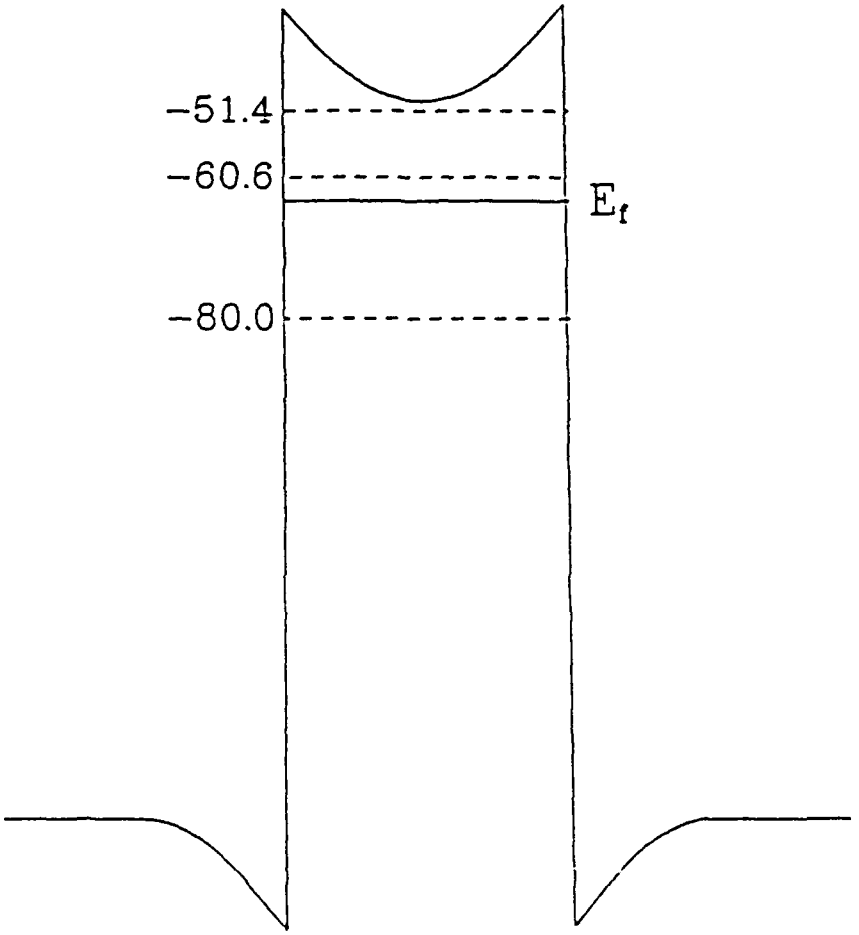

Figure A3 Effective potential, Fermi energy and the highest three confined levels in the doped GaAs/$In_{0.2}Ga_{0.8}As$/GaAs quantum well. The width of the InGaAs layer is 140 Å. The doped layers are symmetrically located on both side of the quantum well and have a width 50 Å with doping density $5x10^{17}$ cm^{-3}. A 20 Å spacer layer separates the doped layer from the quantum well.

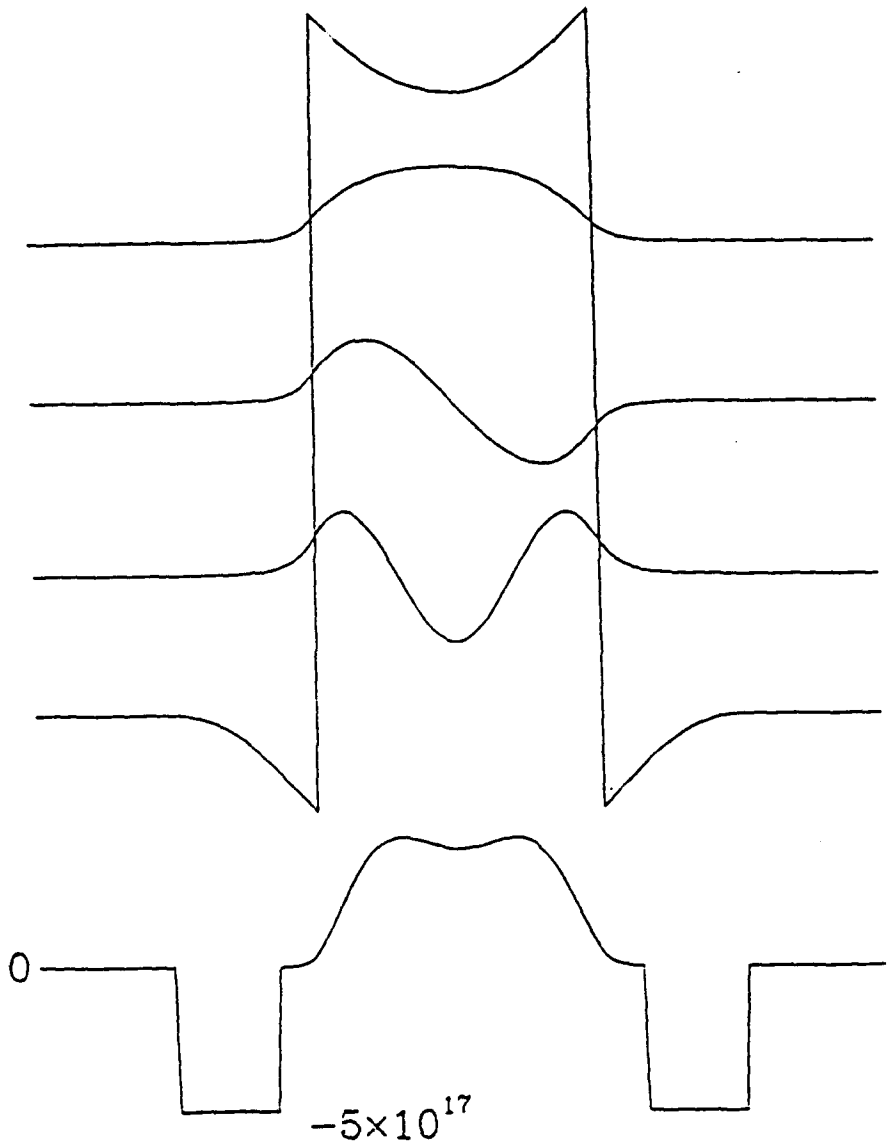

Figure A4 Wave functions and charge density of the doped quantum well. The wave functions of the three confined levels in Figure A3 are shown. The vertical separation between the wave functions is not proportional to the energy scales. The charge distribution is plotted in the lower part of this figure.

has a width of 50 Å with a spacer layer of 20 Å, which separates the doped layer from the edge of the quantum well. A constant doping density 5 x 17 cm^{-3} is assigned for both doped layers. Since the total doped width equals 100 Å, the corresponding two-dimensional doping density (N_{2D}) is 5 x 11 cm^{-2}. The resultant Fermi level has energy slightly lower than the maximum energy of the second subband. (Since the light-hole mixing is neglected in the self-consistent calculation, each subband is a parabolic function of the in-plane wave vector K.)

The envelope functions of the lowest three levels and the equilibrium charge distribution are also plotted in Figure A4. Two constant negative charge regions are the two doped layers. Since the holes flow into the quantum well, the doped layers are left with a negative charge density, $-N_d$. The positive carriers are distributed in the quantum well according to the square of the envelope functions of the occupied levels. The camel-back structure on the top of the carrier distribution indicates the mixture of the second subband which has a node-plane in the center of well and peaks on the sides of the well.

Figure A5 plots the confined level of the zero in-plane wave vector and the profile of the effective potential for an asymmetrically doped quantum well. The charge distribution and the envelope functions of the highest two levels are plotted in Figure A6. In this case, the acceptors are doped only one side of the quantum well. The doped layer has a width of 50 Å and are separated from the edge of the well by a spacer layer of 20 Å. In order to obtain the same two-dimensional carrier density as the symmetrically doped well, the doping density is twice the doping density of the previous case. The resultant Fermi level is only 1 meV lower than the maximum of the second subband; therefore the charge distribution does not show the camel-back structure as in the case of symmetrical doping. The maximum energy of the highest subband falls in potential dip which is similar to the potential in an inversion layer, and the peak of its envelope is moved closer to the doping layer. A stronger interaction between carriers and acceptor may be expected in this case. Another feature of the asymmetric doping is the net potential difference caused by the internal dipole layer. Figures A5 and A6 show that a potential increase of 60 meV as z runs from negative infinity to positive infinity. An applied gate voltage will change the charge distribution, and therefore change the dipole-induced potential difference.

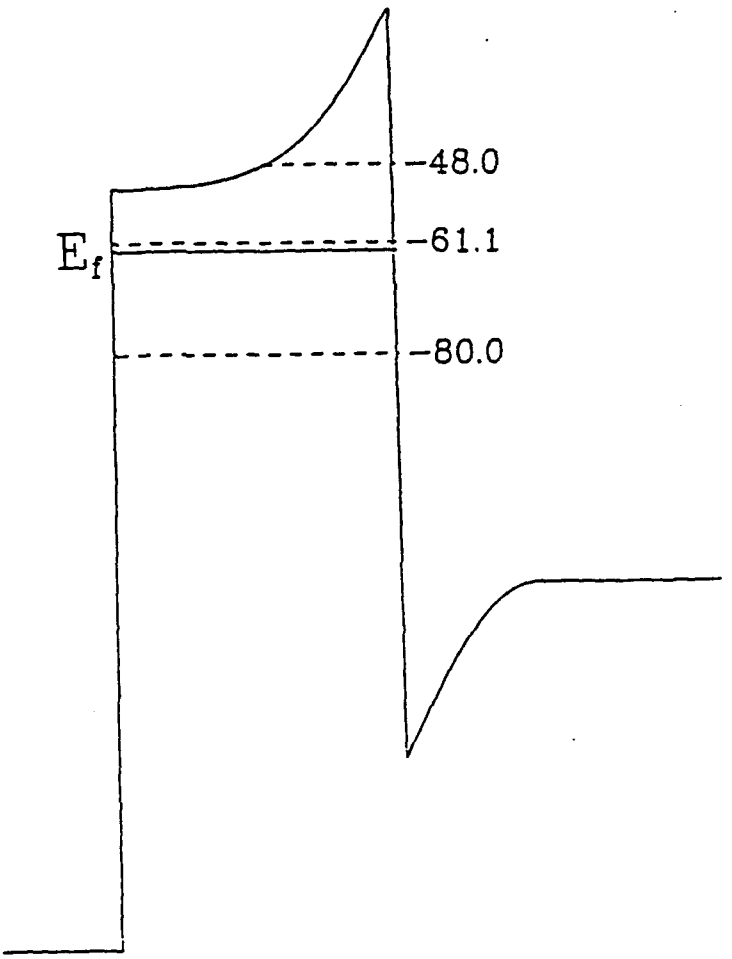

Figure A5 Effective potential, Fermi energy and confined levels of an asymmetrically doped quantum well. The ;width of the InGaAs is the same as that in Figure A3 (140 Å). The doped layer has a width of 50 Å with a doping density 10^{18} cm^{-3} and is located on the right hand side of the well. The doped layer is separated by a 20 Å spacer layer from the quantum well.

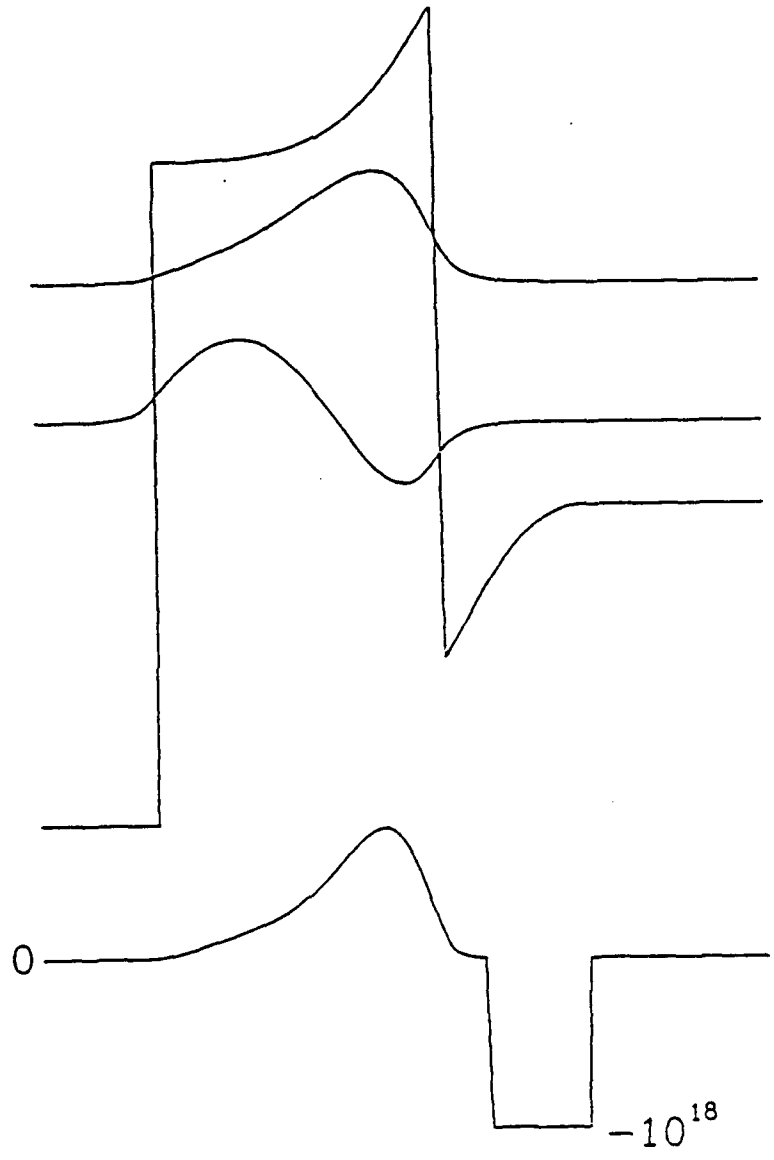

Figure A6 Wave functions and charge density of the asymmetrically doped quantum well. The wave functions of the highest two confined levels in Figure A5 are shown. The charge distribution is plotted in the lower part of this figure.

REFERENCES

A1. M. Weyers, N. Putz, H. Heniecke, M. Heyen, H. Luth, and P. Balk, *J. Electron. Mater.* **15**, 57 (1986).

A2. P. Chu, S. Niki, J.W. Roach, and H.H. Wieder, *Rev. Sci. Instrum.* **58**, 1764 (1987).

A3. C.W. Tu, B.W. Liang, T.P. Chin, and J. Zhang, *J. Vac. Sci. Technol. B* **8**, 293 (1990).

A4. Y.-T. Lu, Ph.D. Thesis, Univ. Calif. San Diego, (1989).

A5. J.M. Luttinger, *Phys. Rev.* **102**, 1030 (1956).

A6. G.E. Bir and G.E. Pikus, *Symmetry and Strain-Induced Effects in Semiconductors* (Wiley, New York, 1974) , p. 238.

APPENDIX B

List of Publications and Conference Presentations

Publications

1. C.W. Tu, B.W. Liang, T.P. Chin, and J. Zhang, "Growth and characterization of GaAs grown by metalorganic molecular-beam epitaxy using trimethylgallium and arsenic," *J. Vac. Sci. Technol. B* **8**, 293 (1990).

2. B.W. Liang, T.P. Chin, and C.W. Tu, "Reflection high-energy electron-diffraction study of metalorganic molecular-beam epitaxy of GaAs using trimethylgallium and arsenic,"*J. Appl. Phys.* **67**, 4393 (1990).

3. B.W. Liang and C.W. Tu, "Surface kinetics of chemical beam epitaxy of GaAs," *Appl. Phys. Lett.* **57**, 689 (1990).

4. C.W. Tu, B.W. Liang, and T.P. Chin, "The effects of arsenic overpressure in metalorganic molecular beam epitaxy of GaAs and InAs," *J. Cryst. Growth* **105**, 195 (1990).

5. B.W. Liang, T.P. Chin, L.Y. Wang, and C.W. Tu, "A study of metal-organic molecular beam epitaxy growth of InAs by mass spectrometry and reflection high-energy electron diffraction," *J. Cryst. Growth* **195**, 240 (1990).

6. B.W. Liang, K. Ha, J. Zhang, T.P. Chin, and C.W. Tu, "Growth of InAs on GaAs(001) by migration enhanced epitaxy," *SPIE Proc.* **1285**, 116 (1990).

7. B.W. Liang, L.Y. Wang, and C.W. Tu, "A kinetic model for metal-organic molecular-beam epitaxy of InAs," *Proc. State-of-the-art Prog. on Comp. Semicond.* **XII** (1990).

8. C.W. Tu, B.W. Liang, and V.M. Donnelly, "Metalorganic molecular-beam epitaxy: growth kinetics and selective-area epitaxy," *Chin. Mat. Res. Soc. Int. '90 Symp. Proc.*, **1**, 511(1990).

9. J. Zhang, N.C. Tien, E.W. Lin, H.H. Wieder, W.H. Ku, C.W. Tu, D.B. Poker, and S.N.G. Chu, "Molecular-beam epitaxial growth and characterization of pseudomorphic modulation-doped field-effect transistors," *Thin Solid Films* **196**,295(1991).

10. T.P. Chin, B.W. Liang, H.Q. Hou, M.C. Ho, C.E. Chang, and C.W. Tu, "Determination of V/III ratios on phosphide surfaces during gas-source molecular-beam epitaxy," *Appl. Phys. Lett.* **58**,254(1991).

11. C.E. Chang, T.P. Chin, and C.W. Tu, "A differential reflection high energy electron diffraction measurement system," *Rev. Sci. Instrum,* **62**,655 (1991).

12. J.C.P. Chang, T.P. Chin, K. Kavanagh, and C.W. Tu, "High-resolution x-ray diffraction of InAlAs/InP superlattices grown by gas-source molecular-beam epitaxy," *Appl. Phys. Lett.* **58**,(1991).

Conference Presentations

1. T.P. Chin, B.W. Liang, C.E. Chang, and C.W. Tu, "Low-cost enhancements to a Varian MBE system," Varian Users' Meeting, San Jose, CA 9/11/89.

2. B.W. Liang, T.P. Chin, and C.W. Tu, "RHEED study of MOMBE growth of GaAs using trimethylgallium and arsenic," 10th US MBE Workshop, Raleigh, NC 9/89.

3. C.W. Tu, B.W. Liang, T.P. Chin, and J. Zhang, "Growth and characterization of GaAs grown by MOMBE using trimethylgallium and arsenic," Second Int. Conf. CBE and Rel. Tech., Houston, TX 12/89.

4. B.W. Liang, T.P. Chin, L.Y. Wang, and C.W. Tu, "A study of MOMBE growth of InAs by mass spectrometry and RHEED," Second Int. Conf. CBE and Rel. Tech., Houston, TX 12/89.

5. C.W. Tu, B.W. Liang, T.P. Chin, and L.Y. Wang, "Growth kinetics of MOMBE of GaAs and InAs," Workshop on Comp. Semicond. Mat. and Devices, San Francisco, CA 2/90.

6. B.W. Liang, K. Ha, J. Zhang, T.P. Chin, and C.W. Tu, "Growth of InAs by migration enhanced epitaxy," SPIE Symp. Growth of Semicond. Struc. and High T_c Thin Films on Semicond., San Diego, CA 3/17-21/90.

7. B.W. Liang, L.Y. Wang, T.P. Chin, and C.W. Tu, "Surface chemical reaction mechanism of metal-organic molecular beam epitaxy (MOMBE) of InAs using trimethylindium (TMIn) and arsenic," APS March Mtg., Anaheim, CA 3/14-17/90.

8. J. Zhang, N.C. Tien, E.W. Lin, H.H. Wieder, W.H. Ku, C.W. Tu, D.B. Poker, and S.N.G. Chu, "Molecular-beam epitaxial growth and characterization of pseudomorphic modulation-doped field-effect transistors," Eighth Int. Conf. Thin Films, San Diego, CA 4/2-6/90.

9. C.W. Tu, B.W. Liang, and V.M. Donnelly, "Metalorganic molecular beam epitaxy: growth kinetics and selective-area epitaxy," Chin. Mat. Res. Soc. Int. 90, Beijing, China 6/18-22/90.

10. C.E. Chang, T.P. Chin, and C.W. Tu, "A differential reflection high energy electron diffraction measurement system," Varian Users' Mtg., La Jolla, CA 8/24/90.

11. T.P. Chin, B.W. Liang, H.Q. Hou, M.C. Ho, C.E. Chang, and C.W. Tu, "Phosphorus-induced growth of GaP, AlP, and InP (100) by gas-source molecular-beam epitaxy," Varian Users' Mtg., La Jolla, CA 8/24/90.

12. B.W. Liang and C.W. Tu, "The roles of group-V species in metal-organic molecular-beam epitaxy of GaAs, InAs, and GaSb," Sixth Int. Conf. MBE, La Jolla, CA 8/27-31/90.

13. C.W. Tu, T.P. Chin, H.Q. Hou, B.W. Liang, and M.C. Ho, "Growth of binary and ternary phosphides by gas-source MBE," Int. Conf. Electron. Mat., Newark, NJ 9/17-19/90.

14. B.W. Liang and C.W. Tu, "The roles of antimony in metal-organic molecular-beam epitaxy of GaSb," 37th AVS Ann. Symp., Toronto, Canada 10/90.

15. T.P. Chin, B.W. Liang, H.Q. Hou, M.C. Ho, and C.W. Tu, "Group-V induced growth of III-V compounds by gas-source MBE," Mat. Res. Soc. Symp. T, 11/26-12/1/90.

 ☆U.S. GOVERNMENT PRINTING OFFICE: 1991 - 548-076/44269